BRIDGING STRUCTURE AND FUNCTION: MAGNETIC RESONANCE IMAGING FOR COMPREHENSIVE BRAIN CONNECTIVITY STUDY

by

WENWU SUN

(Under the Direction of Qun Zhao)

ABSTRACT

This dissertation employs magnetic resonance imaging (MRI) to investigate functional and structural connectivity of in vivo brains. The study involves a range of MRI techniques—functional MRI (fMRI) for brains' temporal dynamics analysis, diffusion tensor imaging (DTI) for structural connectivity mapping, and a machine learning approach for functional/structural data integration and connectome matrix fusion. All MRI data were acquired from brains of a porcine model, which has demonstrated its utility as a surrogate model for studying human brains.

Chapter 2 focuses on using fMRI to study brain recovery mechanisms of post-traumatic brain injury (TBI). A temporal analysis compares TBI subjects with a sham group where only craniotomy surgery was performed to assess brain function recovery. This analysis yields a deeper understanding of brain activity over time enhanced by sparse dictionary learning and independent component analysis. Combined with application of cerebral blood flow mapping, this method introduces a novel approach for evaluating the efficacy of treatments like fecal microbial transplants in TBI recovery, evidenced by increased correlation within the executive control and salience networks.

In Chapter 3, the investigation shifts to DTI to develop a new white matter atlas tract model for piglets. This approach shifts from conventional surface-based methodologies to a voxel-based structural connectivity analysis, providing a detailed view of the brain's organizational complexity. The structural connectome blueprints generated facilitate a deeper comprehension of neurodevelopmental processes and the impact of therapeutic interventions on brain structure.
Chapter 4 synthesizes learnings from the preceding chapters and introduced the Connectome Matrix Fusion methodology. This approach integrates structural and functional connectivity data and provides a comprehensive view of the brain's connectome. The method markedly enhances the differentiation of effect on brains following nutritional interventions, underscoring its significance for neuroscience research.
Chapter 5 summarizes contributions of this dissertation and presents future research directions. The dissertation underscores the pig model's contribution to neurological research by integrating advanced MRI methodologies, laying the groundwork for future studies on brain connectivity and recovery mechanisms. This comprehensive analysis elucidates the brain's structural and functional complexities, advancing our understanding of brain health and disease and setting a new course for neurological research advancements.

INDEX WORDS: Magnetic Resonance Imaging (MRI), Pig Brain Model, Functional MRI (fMRI), Diffusion Tensor Imaging (DTI), Connectome Matrix Fusion, Traumatic Brain Injury (TBI), Sparse Dictionary Learning, Independent Component Analysis, Cerebral Blood Flow Mapping, White Matter Atlas Tract Model, Neurodevelopmental Processes

BRIDGING STRUCTURE AND FUNCTION: MAGNETIC RESONANCE IMAGING FOR COMPREHENSIVE BRAIN CONNECTIVITY STUDY

by

WENWU SUN

BS, Peking University, 2017

A Dissertation Submitted to the Graduate Faculty of The University of Georgia in Partial Fulfillment of the Requirements for the Degree

DOCTOR OF PHILOSOPHY

ATHENS, GEORGIA

2024

BRIDGING STRUCTURE AND FUNCTION: MAGNETIC RESONANCE IMAGING FOR COMPREHENSIVE BRAIN CONNECTIVITY STUDY

by

WENWU SUN

Major Professor:	Qun Zhao
Committee:	Loris Magnani
	Heinz-Bernd Schuttler

Electronic Version Approved:

Ron Walcott
Vice Provost for Graduate Education and Dean of the Graduate School
The University of Georgia
May 2024

ACKNOWLEDGEMENTS

I want to first sincerely thank my advisor, Dr. Qun Zhao. He has always been tolerant of my careless mistakes and delayed reports and supervising me to make progress through this long journey. Not only did he guide my academic growth, but he also solidly supported me through the COVID-19 pandemic and the dark times in my life, helping me become a stronger person. Xiexielaoshi! I also want to thank my advisory committee, Dr. Loris Magnani and Dr. Heinz-Bernd Schuttler, for their consistent support and valuable feedback along the way.

I also want to thank Gregory Simchick for his generous and patient guidance through the learning process and into research. His methodologies and code scripts continue to shine in the lab. I sincerely wish him a happy married life!

I want to extend my gratitude to my fellow friends and collaborators. I am thankful for William Reeves and Ishfaque Ahmed for their academic and emotional support, which meant so much to me. I want to thank Dr. West, Dr. Park, and their fascinating group members. Thanks for their hard work with the pigs to make everything possible. I also want to thank Kim Mason for collecting the data and taking care of everything needed in the BIRC lab. Many thanks to Dr. Inseok Song, Dr. Kanzo Nakayama, Dr. Steven Lewis, and other friendly people in the department too.

Finally, I want to thank my family and friends. Cheers to all of them. Their love is my dearest treasure.

TABLE OF CONTENTS

Page

LIST OF TABLES

Page

LIST OF FIGURES

Page

CHAPTER 1

INTRODUCTION

The human brain, composed of billions of interconnected neurons, remains an attractive object with secrets yet to be unveiled. Over the years, advancements in non-invasive imaging techniques, especially magnetic resonance imaging (MRI), have significantly deepened our understanding of the brain. With different pulse sequences employed, MRI is capable of detecting functional information and structural information in the brain. Specifically, functional magnetic resonance imaging (fMRI) has been used to analyze functional connectivity, capturing the dynamic interactions between distinct brain regions at rest or when they engage in various tasks[1-3]. Diffusion tensor imaging (DTI) maps the brain's structural connectivity by revealing the physical connection between brain regions[4]. There is also a growing interest in integrating both functional and structural MRI together as multi-model study, known as connectivity fusion, that offers more comprehensive understanding and has great potential with brain study[5-7].

While the advanced imaging techniques provide a window into studying the brain's intricate mechanisms, realizing their full potential often requires appropriate models to approximate the human brain, especially in pre-clinical research. Traditionally, rodent and non-human primate models have been preferred for these studies[8-10]. However, these models have notable drawbacks. Rodents, despite their convenience, possess a brain anatomy that significantly diverges from that of humans, thus limiting direct translational implications. The missing of brain gyrus also adds to the difficulty of translating the rodent findings to human findings[11]. On the other hand, non-human primates, while anatomically and functionally closer to

humans, introduce great economic and ethical complexities. Recently, pig stands out as an excellent translational model. The pig model's brain size, structure, composition, and neurodevelopmental trajectory closely mirror those of humans, enhancing the relevance and translational potential of MRI studies conducted on the pig model for understanding human neurobiology[12,13].

Functional Connectivity (FC)

Over the last several decades, functional magnetic resonance imaging (fMRI) has become a predominant methodology for mapping the human brain's functionalities. Functional connectivity describes the synchronized activity between spatially distinct neural regions. Various techniques were developed and employed for functional connectivity measurement and among these, fMRI stands out due to its non-invasive nature, offering high spatial resolution in vivo insights into brain dynamics compared to other techniques (like Positron Emission Tomography (PET), Electroencephalography (EEG), Magnetoencephalography (MEG), etc.)[2,14]. The effectiveness of fMRI and relation between fMRI signal and electrophysiological activation in brain regions was proved by studies on non-human primates[15-17].

Specifically, fMRI captures the variations in brain metabolism, particularly oxygenation, to analyze brain functional connectivity. At the cellular level, neuron activations rely on adenosine triphosphate (ATP) for energy supply. The primary source of ATP is the oxygen-dependent breakdown of glucose, known as Krebs cycle[18]. As specific brain regions become active and ATP is used to provide energy, a higher request for oxygen supply is needed by the circulatory system[19]. This brain region activity will result in oxygen transformation from the blood hemoglobin to the glycolysis, and further results in generating deoxygenated hemoglobin[15,20,21]. Then, higher blood flow is gathered around the activated brain region by

neighboring veins to supply oxygenated hemoglobin. This subsequent hemodynamic response reverses this trend, not only replenishing the oxygen levels but temporarily surpassing them, resulting in a surplus of oxygenated hemoglobin[2,22,23]. Given that deoxygenated hemoglobin is paramagnetic, it induces magnetic field disruptions, leading to dephasing of neighboring water molecules and decreasing MR signal. As the hemodynamic response plays out, concentration of deoxygenated hemoglobin lowers and is transit to its oxygenated state, causing an increase in the MR signal. This phenomenon gives rise to what is commonly referred to as the blood oxygenation level dependent (BOLD) signal in fMRI. To understand these changes, the effects of deoxyhemoglobin concentration change are categorized into two intravascular and two extravascular BOLD effects [24].

For the intravascular parts, the effect of hemoglobin concentration on the relaxation time $T_{2\,BL}^{*}$ is count as KI_{T2BL}, while the effect of phase difference caused by oxygenation related susceptibility is noted as KI_{PH}. Both intravascular parts are introduced by the change in concentration of deoxyhemoglobin. On the other hand, extravascular effects come from the changing field gradients in the microscopic structures and are separated into effects around a straight vein KE_{SV} and capillaries at random orientation KE_{CAP} . The total signal at a given place can be written as

$$S_{total} = \sum_{tissue} \lambda_{tissue} \cdot S_{tissue} \qquad (1.1)$$

Where λ_{tissue} is the volume of each involved tissue. The S_{tissue} can be given as:

$$S_{tissue} = K_{gain} \cdot \rho_{tissue} \cdot \left(1 - \exp\left(-\frac{TR}{T_{1\,tissue}}\right)\right) \cdot \exp\left(-\frac{TE}{T_{2\,tissue}^{*}}\right) \cdot \exp\left(i \cdot \varphi_{tissue}\right) \quad (1.2)$$

where K_{gain} is a location and instrument related gain function, TE is the echo time, ρ_{tissue} stands for the tissue's relative proton density to water, and φ_{tissue}describe phase different

between blood and surrender tissue parts. TR is the repetition time of the scan and $T_{1_{tissue}}$ is the relaxation time specific to each part of tissue.

Specifically, the K_{T2BL} effect on the relaxation time $T_{2\,BL}^{*}$ can be written as[25]:

$$\frac{1}{T_{2\,BL}^{*}} = K_0 + K_1 \cdot (1-Y) + K_2 \cdot (1-Y)^2 + K_{inhom} \quad (1.3)$$

where Y is the oxygenation level in the brain section and K_{inhom} refers to the macroscopic field inhomogeneities. The K_i coefficients are generated from tissue properties and density and are specified for the magnetic field employed for the scan.

Next, the KI_{PH} is given by[3]:

$$\varphi_{BL} = 2\pi \cdot \gamma \cdot \Delta_\chi \cdot Hct \cdot (1-Y) \cdot B_0 \cdot \left(cos^2\theta - \frac{1}{3}\right) \cdot TE \quad (1.4)$$

where γ is the gyromagnetic ratio, Δ_χ is the difference of susceptibility between oxygenated and deoxygenated hemoglobin, and Hct is the mean hematocrit level in blood.

Then, the extravascular effects KE_{SV} can be described as[26]:

$$R2'_{cap} = \frac{3}{4}\pi \cdot \gamma \cdot \Delta_\chi \cdot Hct \cdot \left(1 - Y_{cap}\right) \cdot B_0 \cdot \nu_{BL} \quad (1.5)$$

where ν_{BL} is the fraction of blood in capillaries, and Y_{cap} gives the oxygenation level in the capillaries in gray matter,

And the dephasing around a single vessel KE_{CAP} is given by[3]:

$$\eta = 1 - U(\delta\varpi_\theta \cdot TE) \cdot \frac{\lambda_{BL}}{1-\lambda_{BL}} + U(\lambda_{BL} \cdot \delta\varpi_\theta \cdot TE) \cdot \frac{1}{1-\lambda_{BL}} \quad (1.6)$$

where $\delta\varpi_\theta$ gives the characteristic frequency shift of a vessel at certain degree to the field B. λ_{BL} is the relative blood volume and U is a more detailed biophysical function. $\delta\varpi_\theta$ can be given as[3]:

$$\delta\varpi_\theta = 2\pi \cdot \gamma \cdot \Delta_\chi \cdot Hct \cdot (1-Y) \cdot B_0 \cdot sin^2\theta \quad (1.7)$$

However, the BOLD signal does not offer a straightforward correspondence with neural activities. Instead, it encapsulates a more complex blend of various sources, including synaptic potentials and local field potentials. The signal is affected by the region-specific biophysical parameters and is subject to noise from multiple sources. Furthermore, the signal is spatially spread across the neighboring brain region. Specifically, we have the following equation[16] to describe the BOLD signal and neural activation:

$$B(x) = \int_{n(x)} \big(A(u) + N_N(u)\big) H(u) P(x - u) du + N_M(x) \qquad (1.8)$$

where $B(x)$ is the BOLD signal, and $A(u)$ is the action/stimulus driven neuron activation at space location *u.* $N_N(u)$ refers to the uncontrolled neural responses, $H(u)$ refers to the parameter *Hemodynamic response efficiency (HRE)* which describes the coupling of neural activity and vascular response rate, and $P(x - u)$ refers to the spread of signal, normally at ~5mm scale. Finally, $N_M(x)$ describes the measurement system noise. This is a well-accepted biophysical model to interpret the relationship between BOLD signal and neural activities.

The spatial resolution of the BOLD signal is a blurred representation of the neural activity due to the architecture of the vascular and neural networks. Moreover, the time course of the BOLD response to a brief stimulus (hemodynamic response function, HRF) begins with a delay of about 2 seconds after stimulus onset, peaks between 4 to 6 seconds, and returns to baseline, sometimes undershooting before stabilizing[27]. These temporal dynamics, along with the spatial characteristics of the BOLD signal, shift the focus from considering only spiking activity to appreciating the broader spectrum of neuronal processing reflected in the BOLD signal. Overall, the intricate relationship between the BOLD signal and neuronal activity, influenced by both neurovascular coupling mechanisms and the metabolic demands of neuronal processing, underscores the complexity of interpreting fMRI data. As such, extracting precise information

about neuronal activity patterns from the BOLD signal requires careful consideration of its physiological underpinnings, the spatial and temporal resolution of the imaging technique, and the specific brain region being studied.

When discussing fMRI research, there are generally two primary study types by experiment design: one that involves specific cognitive tasks or stimulation, and aim to identifies correlated brain activation patterns; and the other one conducted while the subject stays at rest and delves into the temporal synchronization of spatially separated regions of interest. It is also common to specify types as task-based (tb-) and resting-state (rs-) fMRI based on the state of brain in studies. As definition, rs-fMRI captures the BOLD signal during periods when no external stimuli or tasks are presented to the subject and reveals intrinsic neural activity correlations. These activities are believed to be associated with complex neuronal processes that continuously operate in the background, encompassing facets like self-awareness, emotion, and memory.[28-31]

Broadly, the methodologies employed in functional connectivity studies via fMRI fall under two categories: seed-based (model-based) and data-driven (modal-free) approaches[32]. The former, like cross-correlation analysis (CCA), are rooted in prior knowledge and are popular due to their simplicity. In contrast, data-driven strategies function without pre-existing knowledge, making them particularly valuable for resting-state fMRI where patterns are often unknown. Recent shifts in research paradigms are focusing less on the singular activated brain regions and more on how these distinct areas collaboratively work to facilitate specific cognitive functions.

Seed-based methodology

A significant portion of functional connectivity research has employed a seed-based approach. In these studies, specific regions of interest (ROIs) are chosen as "seeds." The

connectivity between these seeds and other brain regions is then determined by applying predefined metrics, resulting in a connectivity map of the brain. The simplicity and effectiveness of defining ROIs make seed-based methodologies widely employed. However, such methods often rely heavily on well-established neuroscience knowledge or empirical experience and is hard to apply on new protocols. Depending on the metrics adopted to measure connectivity, these model-based methods can be further categorized as follows:

Cross-correlation analysis

Cross-correlation analysis (CCA), a well-established technique, has found applications across diverse fields. Its introduction to functional connectivity MRI (fcMRI) research was pioneered by Cao and Worsley[33]. This technique operates on the premise that when a specific region of the brain is functionally linked to a designated seed, their respective BOLD time courses exhibit correlation. By evaluating variance across different regions, cross-correlation analysis gauges the synchronicity of these BOLD time series. However, there are challenges to this methodology: Firstly, correlation is acutely sensitive to the Hemodynamic Response Function (HRF), which has variations across subjects and even within different regions of the same brain [34]. Secondly, high correlations can arise due to noise sources, such as cardiac and blood vessel activity in the brain, creating fake significant correlation[35].

Coherence analysis

To navigate these challenges, Sun et al. [36] introduced a novel metric: coherence, which is defined as the spectral representation of correlation within the frequency domain. Coherence offers a different view of connectivity. Techniques such as the Short Time Fourier Transform (STFT), Continuous Wavelet Transform, and Empirical Mode Decomposition (EMD) are

commonly leveraged extensions of coherence. Yaesoubi et al. [37] also brought up a framework for dynamic coherence analysis of resting state fMRI.

This shift to the frequency domain provides researchers with a new framework to assess the relationship dynamics of time series. For instance, fluctuations in blood flow typically cycle around every 10 seconds. This means that coherence at frequencies below 0.1 Hz can be possibly noted as noise. Similarly, since the heart bumps at a frequency close to 1.25 Hz, coherence in this frequency range might be attributed to cardiac activity rather than brain functional connectivity. Emphasizing frequency domain analysis can therefore discern between these different physiological phenomena[32], which causes problem with CCA.

Data-driven methodology

To address the shortcomings associated with model-based approaches, various methodologies that don't rely on predetermined seeds or prior knowledge have been introduced. Functional connectivity detection can be achieved through decomposition techniques, including but not limited to principal component analysis (PCA), independent component analysis (ICA), clustering methods, and graph theoretical approaches[38]. These techniques aim to represent the fMRI data set through a series of basis vectors (in the case of PCA and SVD) or independent components (as seen in ICA). FC patterns can also be detected thru clustering analyses, such as fuzzy clustering analysis (FCA) and hierarchical clustering analysis (HCA). Both types provide comprehensive insights into the brain's functional connectivity.

Principal component analysis (PCA)

Principal component analysis (PCA) is a prominent method for data interpretation. This technique focuses on expressing observed fMRI time series through a combination of orthogonal components characterized as unique temporal pattern (a principal component) and corresponding

spatial pattern (an eigen map of each component at each voxel of the brain)[32]. The resulting eigen maps identify regions with correlation as showing high absolute values. However, PCA faces challenges to identify correct components, particularly when other sources of signal variation such as physiological noise are present[39]. It is also hard to fine tune the proper number of components employed. Thus, PCA is seldomly used alone in resting-state analyses but can help in preprocessing steps, where components contributing minimally to data variance are discarded to refine the signal data while preserving most of the signal power.

Independent component analysis (ICA)

Independent component analysis (ICA) is a computational method that separates a multivariate signal into additive, independent non-Gaussian components. Similar to PCA, it decomposes time series signals to components and calculates corresponding eigen maps as spatial patterns. However, as PCA finds orthogonal components, ICA seeks for components that are as statistically independent as possible[32,40]. For example, for two unit-vectors (*v1, v2)* that are not orthogonal, PCA will decompose them into orthogonal coordinates and corresponding coefficients, while ICA will find *v1 and v2* as the components. In the context of fMRI, ICA is used to identify spatially independent patterns of brain activity that occur simultaneously, revealing functionally connected networks without the need for a priori knowledge of the ROIs. Mathematically, ICA can be written as:

$$X = AC, or\ X = \sum_{i=1}^{N} A_i C_i \qquad (1.9)$$

$$C = WX \qquad (1.10)$$

where *X* is the fMRI signal matrix of time series *T* by number of voxels *N*. *A* is the mixing matrix and C is the component matrix storing all independent components. *W* (unmixing matrix) is the pseudo reverse of *A* and is used to obtain the independent components [41,42]. In practice, due to

the invention of dual-regression [43,44], a procedure capable of regressing eigenvalue maps, or activation maps, to the signal domain, decomposition of the time domain (tICA) and of the spatial domain (sICA) are both widely used. The choice Is often made by considering the temporal and spatial feature of the underlying simulation/activation pattern. Overall, ICA performs better in feature detection [32,45], but also suffers from fine tuning the component number and rely on the assumption that the components are independent..

Functional connectivity methods

After employing seed-based or data-driven signal processing, features of brain functional activities are extracted from the raw fMRI data. Subsequently, various methods are utilized to explore the functional connectivity of ROIs throughout the brain. These methods include hierarchical clustering, graph theory models, and several other analytical techniques, enabling a comprehensive examination of brain network organization and interactions among different brain regions.

Hierarchical clustering

In fMRI studies, clustering analysis techniques such as fuzzy clustering, vector quantization, self-organizing maps, and neural gas networks have been extensively utilized to identify patterns of functional connectivity. The core objective is to group sufficiently similar ROIs into clusters based on the similarity of their corresponding time series. However, these clustering methods are having fixed number of clusters to fit in. On the other hand, hierarchical clustering analysis begins by treating each ROI as an individual cluster and progressively merges clusters based on a specific distance measure[46]. This procedure effectively concludes information from the entire dataset. By how it measures closeness and different type of distance calculation employed, there are variations like single-linkage, complete-linkage, and average-linkage

clustering. FSLNETs is a well-accepted framework of FC study utilizing hierarchical clustering with time series from dual regression procedure for each ROI identified by ICA and is referenced and utilized in chapter 1[47]. Despite its potential for better detailed analysis, hierarchical clustering is computationally demanding.

Graph theory models

Graph analytical methods are another family that is built to deal with connectivity studies. These methods treat the human brain as a single, complex network integrating all ROIs and sub-networks into a comprehensive system. Investigating the overall organization of this network can provide valuable insights into the brain's operation, including the organization of functional connections, the efficiency of information integration across sub-systems, and the identification of crucial dominant regions. Graph theory offers a framework to analyze the topology of these complex networks, shedding light on both local and global organizational aspects of functional connectivity studies.

In graph theory, functional brain networks are normally depicted as graphs $G = (V, E)$, where V represents brain regions (nodes) and E denotes the functional connections (edges) between nodes. This framework allows the nodes to represent neighboring cortical areas. The functional connectivity level between regions is measured by the correlation of their time series, with the overall network's organization examined through various graph metrics. Key graph properties, including clustering coefficient, characteristic path length, node degree and distribution, centrality, and modularity, offer insights into the network's structure[48,49]. These metrics help understand the network's local connectedness, global connectivity, hub formation, and sub-network integration, potentially identifying networks as small-world, scale-free, or modular. As graph theory becomes increasingly applied to neuroimaging data, new measures are being

developed and evaluated for their ability to analyze the brain's functional and structural connectome, marking a growing field of research with significant implications for understanding brain organization.

Structural Connectivity (SC)

Structural connectivity, in contrast, delves into the anatomical pathways that link different brain regions utilizing MRI. By understanding the structural connections, researchers gain insights into the brain's foundational layout and anatomical information. This perspective becomes crucial when studying developmental patterns, brain injuries, or degenerative diseases where structural anomalies might influence functional outcomes.

The brain consists of massive neural cells and glial cells about 10 times the number of neural cells. In the grey matter, the neural cells are distributed without a uniform direction, leading to isotropic and homogeneous anatomical properties. On the other hand, white matter contains axonal bundles, which are elongated extensions from neural cells designed for electrical pulse transmission. Those bundles exhibit distinct directional orientations, and those orientations can be presented by macroscopic molecule movements with corresponding directions, such as water molecule diffusion. Water molecules move or diffuse more rapidly along white matter fiber bundles compared to their motion perpendicular to these fibers. This anisotropic diffusion is a key characteristic of white matter. A modern non-invasive technique to detect water molecule diffusion is via a diffusion MRI[50] leverages water molecule diffusion to create contrast in MRI images. This contrast offers insights into the Brownian motion of molecules, within biological tissues including gray matter (GM), white matter (WM), and cerebrospinal fluid (CSF) in a non-invasive, in vivo manner. The technique is sensitive to the cellular environment, which influences water mobility; in GM areas where there's little to no constraint, water diffuses

isotopically. In contrast, in WM where bundles exist, diffusion becomes anisotropic and reflects the bundle properties and enabling the detection of pathological changes.

To quantify diffusion parameters that depend on the white matter fiber direction and diameter, an initial scan with no diffusion-sensitizing gradients or with a very low b-value is collected to serve as a reference B_0image. Subsequent diffusion-weighted images (DWI) are acquired at various gradient directions to calculate water molecule diffusion directions. Multiple gradient directions and field strength is utilized for DWI collecting to capture diffusion directions and increase signal to noise ratio. Different DWIs act as decomposition of the brain diffusion map. The phase accumulation with a gradient field G applied with short time δ at place r_0 is[51]:

$$\varphi = \gamma G \delta r_0 \qquad (1.11)$$

where γ is the gyromagnetic ratio. Then after the diffusion happens, when the gradient field is again applied, the phase accumulation at place r_Δ is

$$\Delta\varphi = \gamma G \delta r_\Delta \qquad (1.12)$$

If we note $\gamma G \delta = q$, then

$$\Delta\varphi = q \cdot r \qquad (1.13)$$

And macroscopic MRI signal can be written as

$$M = \int P(r,t) e^{iq \cdot r}\, dr \qquad (1.14)$$

where $P(r,t)$ is the possibility contribution of a molecule at displacement r after time t, and can be derived from Fourier transform through multiple q values and related MRI signals.

To interpret DWI signals, multiple models have been developed including diffusion tensor imaging (DTI), neurite orientation dispersion and density imaging (NODDI), and many alikes. DTI is based on the tensor interpretation at each voxel, while NODDI separate diffusion

into three parts: free water, intercellular, and extracellular, and requires more scans than DTI[52]. Overall, DTI remains the most popular and wide accepted structural MRI method.

Diffusion tensor imaging (DTI)

Diffusion Tensor Imaging (DTI)[53], is a pivotal model in neuroimaging for characterizing the microstructure of brain white matter. DTI uniquely represents each voxel within the brain as a diffusion tensor. This approach captures the directional dependence of water diffusion in white matter, where water molecule movement is significantly restricted perpendicular to the white matter fiber axis, while remaining relatively free along the axis. By calculating tensor anisotropy measures—ratios derived from the tensor's eigenvalues—DTI quantifies the diffusion and offer insights into the brain's directional anisotropy. Through DTI, researchers can infer the structural organization and integrity of white matter pathways, significantly advancing understanding of brain structure and function[54].

The main metrics calculated in DTI analysis are apparent diffusion coefficient (ADC) aka mean diffusivity (MD), fractional anisotropy (FA), axial diffusivity (AD) and radial diffusivity (RD). The MD measures the diffusivity, or moving freedom, of water molecules at a given voxel, and AD and RD gives axial and radial (orthogonal to axial) diffusivity. Fractional anisotropy measures the dependence of direction of diffusion, also known as anisotropy. In a tensor model where the eigen vectors of a voxel can be denoted as λ_1, λ_2, and λ_3 with λ_1 for the axial and λ_2 and λ_3 orthogonal to λ_1, the above metrics can be calculated as[55]:

$$ADC = MD = \frac{\lambda_1+\lambda_2+\lambda_3}{3} \qquad (1.15)$$

$$AD = \lambda_1; RD = \frac{\lambda_2+\lambda_3}{3} \qquad (1.16)$$

$$FA = \frac{\sqrt{3[(\lambda_1-\lambda)^2+(\lambda_2-\lambda)^2+(\lambda_3-\lambda)^2]}}{\sqrt{2(\lambda_1^2+\lambda_2^2+\lambda_3^2)}}, where\ \lambda = \frac{\lambda_1+\lambda_2+\lambda_3}{3} = MD \qquad (1.17)$$

Structural connectivity

Following the vector interpretation of the brain, structural connectivity, or tractography, can be investigated by finding streamlines in the brain. This involves two main methods: deterministic streamlines and probabilistic streamlines. The deterministic streamlines approach utilizes DTI map tensors to deterministically map white matter pathways. Typical methods like the fiber assignment by continuous tracking (FACT) algorithm initiate from a chosen seed point and follow the fiber direction to take small, fixed steps until reaching a termination criterion—typically areas of low fractional anisotropy or when sharp unreasonable direction change occurs[56]. These deterministic approaches uniquely define trajectories based on the seed point, tracing pathways that align with known white matter routes. However, a crucial problem arises as the DTI voxel size and resolution are normally way larger than the microscopic white matter structure sizes. This will result in multiple direction of tracts in a single voxel, and cause problems with the step to take. To address this issue, the probabilistic streamlines algorithms estimate the distribution of potential pathways from the seed region, rather than providing a certain best-guess from the eigenvector. These algorithms utilize the local fiber orientation probability density function (PDF) to guide stepwise streamline propagation, allowing for a more nuanced representation of likely fiber paths by generating thousands of streamlines[57]. Integrated with tract-editing techniques, the probabilistic approach offers a more comprehensive understanding of the distribution of likely pathways, though it remains subject to the limitations inherent in streamline-based methods.

Yet, tractography is not without its challenges, notably the risk of false positive connections, such as streamlines making unreasonable links. Setting inclusion and exclusion

regions help mitigate these issues by incorporating anatomical knowledge to refine the generated tracts, enhancing the reliability of the tractography results.

Through streamline algorithms, structural connectivity between ROIs can be measured be setting the starting and determination seeds both as ROIs to get the connectivity matrix. Other applications including connectome blueprint, which combines tract information and connectivity matrix to form a tract by ROI study, as mentioned in chapter 3.

Fusion of Functional and Structural Connectivity

Current perspectives in neuroscience emphasize that cognitive functions, such as vision, motion, memory, are generated by medium to large-scale networks comprising various brain regions. Describing and studying brain function involves a "network analysis" that explores spatial and temporal relationships among network elements or nodes. This approach differentiates with studies utilizing just structural or functional connectivity but employs both modals together and reflects the structural and functional interrelationships between edges and nodes.

While FC remains fast development and provides massive information about the intrinsic connections of ROIs, a significant challenge with FC analysis is the exponentially increase of number of edges with the number of ROIs involved. This huge number makes reliable and significant connectivity analyses difficult. On the other hand, SC analyses are dealing with sparse matrices due to the nature of physical connection, and they can help with limiting the number of FC edges to be considered by suggesting that the existence of a strong SC edge makes a FC edge more likely.

Multiple models have been developed to genuinely connect the FC and SC, including biophysical models and machine learning models. The biophysical models are trying to find and

interpret the intrinsic relationship between SC and FC, and to build the bridge between physical connections and temporal correlations. The biophysical models to explain intrinsic relationship between SC and FC are listed in the Table 1.1.

In contrast, machine learning models prioritize the efficacy of data integration and pattern identification within connectome datasets. While these models excel at predictive accuracy and the identification of complex patterns in large-scale data, they often do not directly encode the underlying physical or physiological mechanisms. Machine learning models are mainly used as a classifier of normal and disease infected brains. Some studies with variant modality used for neurological disorder detection are listed in Table 1.2.

Nevertheless, it is noteworthy that the applicability of these results to studies of the porcine brain remains unexplored. The pig brain, with its notable anatomical and functional similarities to the human brain, presents a unique opportunity for advancing our understanding of neurophysiological processes. The translation of these models from human to pig brain studies could potentially unveil novel insights into neural connectivity and pave the way for groundbreaking developments in comparative neuroscience.

Overall, MRI technology is a forefront approach in leveraging the pig brain as a valuable model for human neurological research. By employing functional MRI for temporal analysis, structural MRI including diffusion tensor imaging (DTI) for spatial mapping, and innovative techniques for connectome matrix fusion, comprehensive insights into brain activity, recovery processes, and connectivity have been achieved. This multi-modal exploration not only advances our understanding of neurological mechanisms but also highlights the pig brain model's potential in contributing significantly to future neurological studies. Through these methodologies, the

research underscores the promise of MRI technologies in offering a holistic view of brain connectivity and function, paving the way for further discoveries in neuroscience.

REFERENCES

1. Friston KJ, Jezzard P, Turner R. Analysis of functional MRI time-series. Human brain mapping 1994;1(2):153-171

2. Glover GH. Overview of functional magnetic resonance imaging. Neurosurgery Clinics 2011;22(2):133-139

3. Ogawa S, Menon R, Tank DW, et al. Functional brain mapping by blood oxygenation level-dependent contrast magnetic resonance imaging. A comparison of signal characteristics with a biophysical model. Biophysical journal 1993;64(3):803-812

4. Assaf Y, Pasternak O. Diffusion tensor imaging (DTI)-based white matter mapping in brain research: a review. Journal of molecular neuroscience 2008;34(51-61

5. Zhang L, Wang L, Gao J, et al. Deep fusion of brain structure-function in mild cognitive impairment. Medical image analysis 2021;72(102082

6. Rykhlevskaia E, Gratton G, Fabiani M. Combining structural and functional neuroimaging data for studying brain connectivity: a review. Psychophysiology 2008;45(2):173-187

7. Damoiseaux JS, Greicius MD. Greater than the sum of its parts: a review of studies combining structural connectivity and resting-state functional connectivity. Brain structure and function 2009;213(525-533

8. Semple BD, Blomgren K, Gimlin K, et al. Brain development in rodents and humans: Identifying benchmarks of maturation and vulnerability to injury across species. Progress in neurobiology 2013;106(1-16

9. Herculano-Houzel S. The human brain in numbers: a linearly scaled-up primate brain. Frontiers in human neuroscience 2009;3(857

10. Azevedo FA, Carvalho LR, Grinberg LT, et al. Equal numbers of neuronal and nonneuronal cells make the human brain an isometrically scaled-up primate brain. Journal of Comparative Neurology 2009;513(5):532-541

11. Paredes MF, Sorrells SF, Garcia-Verdugo JM, et al. Brain size and limits to adult neurogenesis. Journal of Comparative Neurology 2016;524(3):646-664

12. Simchick G, Shen A, Campbell B, et al. Pig brains have homologous resting-state networks with human brains. Brain connectivity 2019;9(7):566-579

13. Benn RA, Mars RB, Xu T, et al. Opening the Pig to Comparative Neuroimaging: A Common Space Approach Contextualizes the Pig and Human Structural Connectome. bioRxiv 2020;2020.10. 13.337436

14. Shmuel A, Yacoub E, Chaimow D, et al. Spatio-temporal point-spread function of fMRI signal in human gray matter at 7 Tesla. Neuroimage 2007;35(2):539-552

15. Gauthier CJ, Fan AP. BOLD signal physiology: models and applications. Neuroimage 2019;187(116-127

16. Logothetis NK, Wandell BA. Interpreting the BOLD signal. Annu Rev Physiol 2004;66(735-769

17. Shmuel A, Yacoub E, Pfeuffer J, et al. Sustained negative BOLD, blood flow and oxygen consumption response and its coupling to the positive response in the human brain. Neuron 2002;36(6):1195-1210

18. Cisneros-Mejorado A, Pérez-Samartín A, Gottlieb M, et al. ATP signaling in brain: release, excitotoxicity and potential therapeutic targets. Cellular and molecular neurobiology 2015;35(1-6

19. Buxton RB, Frank LR. A model for the coupling between cerebral blood flow and oxygen metabolism during neural stimulation. Journal of cerebral blood flow & metabolism 1997;17(1):64-72

20. Ogawa S, Lee T-M, Kay AR, et al. Brain magnetic resonance imaging with contrast dependent on blood oxygenation. proceedings of the National Academy of Sciences 1990;87(24):9868-9872

21. Ogawa S, Lee TM, Nayak AS, et al. Oxygenation-sensitive contrast in magnetic resonance image of rodent brain at high magnetic fields. Magnetic resonance in medicine 1990;14(1):68-78

22. Buxton RB, Wong EC, Frank LR. Dynamics of blood flow and oxygenation changes during brain activation: the balloon model. Magnetic resonance in medicine 1998;39(6):855-864

23. Davis TL, Kwong KK, Weisskoff RM, et al. Calibrated functional MRI: mapping the dynamics of oxidative metabolism. Proceedings of the National Academy of Sciences 1998;95(4):1834-1839

24. Hoogenraad F, Pouwels P, Hofman M, et al. Quantitative differentiation between BOLD models in fMRI. Magnetic Resonance in Medicine: An Official Journal of the International Society for Magnetic Resonance in Medicine 2001;45(2):233-246

25. Wright GA, Hu BS, Macovski A. Estimating oxygen saturation of blood in vivo with MR imaging at 1.5 T. Journal of Magnetic Resonance Imaging 1991;1(3):275-283

26. Yablonskiy DA, Haacke EM. Theory of NMR signal behavior in magnetically inhomogeneous tissues: the static dephasing regime. Magnetic resonance in medicine 1994;32(6):749-763

27. Buxton RB, Uludağ K, Dubowitz DJ, et al. Modeling the hemodynamic response to brain activation. Neuroimage 2004;23(S220-S233

28. Biswal B, Zerrin Yetkin F, Haughton VM, et al. Functional connectivity in the motor cortex of resting human brain using echo-planar MRI. Magnetic resonance in medicine 1995;34(4):537-541

29. Shen HH. Resting-state connectivity. Proceedings of the National Academy of Sciences 2015;112(46):14115-14116

30. Damoiseaux JS, Rombouts SA, Barkhof F, et al. Consistent resting-state networks across healthy subjects. Proceedings of the national academy of sciences 2006;103(37):13848-13853

31. Uddin LQ, Supekar K, Menon V. Reconceptualizing functional brain connectivity in autism from a developmental perspective. Frontiers in human neuroscience 2013;7(458

32. Li K, Guo L, Nie J, et al. Review of methods for functional brain connectivity detection using fMRI. Computerized medical imaging and graphics 2009;33(2):131-139

33. Cao J, Worsley K. The geometry of correlation fields with an application to functional connectivity of the brain. The annals of applied probability 1999;9(4):1021-1057

34. Buckner RL, Koutstaal W, Schacter DL, et al. Functional–anatomic study of episodic retrieval: II. Selective averaging of event-related fMRI trials to test the retrieval success hypothesis. Neuroimage 1998;7(3):163-175

35. Friston KJ, Holmes AP, Worsley KJ, et al. Statistical parametric maps in functional imaging: a general linear approach. Human brain mapping 1994;2(4):189-210

36. Sun FT, Miller LM, D'esposito M. Measuring interregional functional connectivity using coherence and partial coherence analyses of fMRI data. Neuroimage 2004;21(2):647-658

37. Yaesoubi M, Allen EA, Miller RL, et al. Dynamic coherence analysis of resting fMRI data to jointly capture state-based phase, frequency, and time-domain information. Neuroimage 2015;120(133-142

38. Van Den Heuvel MP, Pol HEH. Exploring the brain network: a review on resting-state fMRI functional connectivity. European neuropsychopharmacology 2010;20(8):519-534

39. Baumgartner R, Ryner L, Richter W, et al. Comparison of two exploratory data analysis methods for fMRI: fuzzy clustering vs. principal component analysis. Magnetic Resonance Imaging 2000;18(1):89-94

40. Oja E, Hyvarinen A. Independent component analysis: algorithms and applications. Neural networks 2000;13(4-5):411-430

41. Hyvärinen A, Oja E. Independent component analysis: algorithms and applications. Neural networks 2000;13(4-5):411-430

42. Calhoun VD, Liu J, Adalı T. A review of group ICA for fMRI data and ICA for joint inference of imaging, genetic, and ERP data. Neuroimage 2009;45(1):S163-S172

43. Beckmann CF, Mackay CE, Filippini N, et al. Group comparison of resting-state FMRI data using multi-subject ICA and dual regression. Neuroimage 2009;47(Suppl 1):S148

44. Nickerson LD, Smith SM, Öngür D, et al. Using dual regression to investigate network shape and amplitude in functional connectivity analyses. Frontiers in neuroscience 2017;11(115

45. Beckmann CF, DeLuca M, Devlin JT, et al. Investigations into resting-state connectivity using independent component analysis. Philosophical Transactions of the Royal Society B: Biological Sciences 2005;360(1457):1001-1013

46. Cordes D, Haughton V, Carew JD, et al. Hierarchical clustering to measure connectivity in fMRI resting-state data. Magnetic resonance imaging 2002;20(4):305-317

47. Smith SM, Nichols TE, Vidaurre D, et al. A positive-negative mode of population covariation links brain connectivity, demographics and behavior. Nature neuroscience 2015;18(11):1565-1567

48. Ahmed I, Reeves WD, Sun W, et al. Nutritional supplement induced modulations in the functional connectivity of a porcine brain. Nutritional Neuroscience 2024;27(2):147-158, doi:10.1080/1028415X.2023.2166803

49. Reeves WD, Ahmed I, Jackson BS, et al. Characterization of Resting-State Functional Connectivity Changes in Hypertension by a Modified Difference Degree Test. Brain Connectivity 2023;13(9):563-573

50. Le Bihan D, Mangin JF, Poupon C, et al. Diffusion tensor imaging: concepts and applications. Journal of Magnetic Resonance Imaging: An Official Journal of the International Society for Magnetic Resonance in Medicine 2001;13(4):534-546

51. Minati L, Węglarz WP. Physical foundations, models, and methods of diffusion magnetic resonance imaging of the brain: A review. Concepts in Magnetic Resonance Part A: An Educational Journal 2007;30(5):278-307

52. Zhang H, Schneider T, Wheeler-Kingshott CA, et al. NODDI: practical in vivo neurite orientation dispersion and density imaging of the human brain. Neuroimage 2012;61(4):1000-1016

53. Basser PJ, Pajevic S, Pierpaoli C, et al. In vivo fiber tractography using DT-MRI data. Magnetic resonance in medicine 2000;44(4):625-632

54. Jbabdi S, Sotiropoulos SN, Savio AM, et al. Model-based analysis of multishell diffusion MR data for tractography: How to get over fitting problems. Magnetic resonance in medicine 2012;68(6):1846-1855

55. Wen J. Structural and microstructural neuroimaging for diagnosis and tracking of neurodegenerative diseases. Sorbonne université: 2019.

56. Mori S, Van Zijl PC. Fiber tracking: principles and strategies–a technical review. NMR in Biomedicine: An International Journal Devoted to the Development and Application of Magnetic Resonance In Vivo 2002;15(7-8):468-480

57. Behrens TE, Berg HJ, Jbabdi S, et al. Probabilistic diffusion tractography with multiple fibre orientations: What can we gain? neuroimage 2007;34(1):144-155

Biophysical model	Description	Application
Simultaneous autoregressive(Valdés-Sosa, Sánchez-Bornot et al. 2005) (Messé, Rudrauf et al. 2015)	Statistical model for spatial correlation; interprets how a variable is linearly related to its neighbors in a spatial grid.	Applied to neuronal data to determine spatial interactions; useful in brain imaging analysis.
Wilson-Cowan (Deco, Jirsa et al. 2009, Bressloff 2010)	Differential equations model the average firing rates of interconnected excitatory and inhibitory neuron populations.	Studies the dynamic behavior of large-scale brain activity and the transitions between different brain states.
Rate fluctuation (Cabral, Hugues et al. 2012)	Capture the variations in the firing rate due to intrinsic noise and the probabilistic nature of neuron firing.	Useful for understanding the variability in neural responses and spontaneous brain activity patterns.
Kuramoto (Cabral, Hugues et al. 2011)	Describes synchronization in a network of coupled oscillators with individual natural frequencies.	Applied to neurons to study phase synchronization, important in cognitive tasks and rhythms like alpha waves.
Fitzhugh-Nagumo (Ghosh, Rho et al. 2008)	Simplified version of the Hodgkin-Huxley model, capturing excitability with two variables representing voltage and recovery.	Used to model action potentials in neurons and analyze the conditions for excitability and oscillations.
Neural mass (Honey, Sporns et al. 2009)	Represents the collective dynamics of large neuronal populations, simulating EEG-like signals from cortical columns	Designed to match the macroscopic electrical activity of the brain, predicting EEG and MEG signals.
Spiking(Deco and Jirsa 2012)	Detailed models that simulate the timing of action potentials, incorporating ion channel kinetics and synaptic interactions	Employed for precise simulations of individual neuronal activity and synaptic transmission.

Table 1.1 Summary of Biophysical Models in Neuroscience Research

Modality	Description	Application
MRI + DTI + fMRI(Dyrba, Grothe et al. 2015)	Uses a combination of imaging techniques with a Region of Interest (ROI)-based approach and a multi-kernel Support Vector Machine (SVM) for classification.	Differentiating Alzheimer's Disease (AD) from normal controls (NC)
MRI + PET + biomarkers(Cheng, Doecke et al. 2015)	ROI-based analysis with domain transfer SVM, integrating multi-modal data.	Classifying Mild Cognitive Impairment (MCI) and differentiating between progressive MCI (pMCI) and stable MCI (sMCI).
MRI + PET(Shi, Zheng et al. 2017)	ROI-based multimodal Sparse Discriminative Pattern Network (SDPN).	Effective in classifying various stages of Alzheimer's progression.
MRI + PET + biomarkers + Genetics(Tong, Gray et al. 2017)	Utilizes a nonlinear graph-fusion approach to integrate multimodal data for classification.	Targets AD diagnosis incorporating genetic information.
MRI + DTI(Aderghal, Khvostikov et al. 2018)	Focuses on the hippocampus using Convolutional Neural Networks (CNN) and transfer learning	Differentiating between AD, MCI, and NC.
MRI + PET + Genetics(Liu, Wu et al. 2019)	Combines structured sparsity and kernel representation methods.	Integrating genetic data for enhanced AD classification accuracy.

Table 1.2 Summary of Multimodal Machine Learning Studies in Neurological Disorder Classification

CHAPTER 2

Evaluation of brain function recovery after traumatic brain injury treatment in a porcine model by cross-group temporal-spatial correlation analysis[1]

[1] Sun, W., Reeves, W., Fagan, M.M., Welch, C.B., Scheulin, K.M., Sneed, S.E., Callaway, T.R., Duberstein, K.J., West, F.D., and Zhao, Q. submitted to *Neurotrauma Reports*, April 2024

Abstract

Traumatic Brain Injury (TBI), a significant global health issue, is affecting approximately 69 million annually. To better understand TBI's impact on brain function and assess the efficacy of treatments, this study employs a novel temporal-spatial cross-group approach with a porcine model, integrating resting-state functional magnetic resonance imaging (rs-fMRI) for temporal and arterial spin labeling (ASL) for spatial information. Our research utilized eighteen 4-week-old pigs divided into 3 groups: TBI treated with saline (SLN, n=6), TBI treated with fecal microbial transplant (FMT, n=6), and a sham group (Sham, n=6) with only craniectomy surgery as the baseline. By applying machine learning techniques—specifically, independent component analysis and sparse dictionary learning—across seven identified resting-state networks (RSNs), we assessed the temporal and spatial correlations indicative of treatment efficacy. Both temporal and spatial analysis revealed a consistent increase of correlation between the FMT and Sham groups in the executive control and salience networks. Our results are further evidenced by a simulation study designed to mimic the progression of TBI severity through the introduction of variable Gaussian noise to an independent rs-fMRI dataset. The results demonstrate a decreasing temporal correlation between sham and TBI groups with increasing injury severity, consistent with the experimental results. This study underscores the effectiveness of the methodology in evaluating post-TBI treatments such as the FMT. By presenting comprehensive experimental and simulated data, our research contributes significantly to the field and opens new paths for future investigations into TBI treatment evaluations.

Introduction

Traumatic brain injury (TBI) is a significant global health issue, affecting approximately 69 million people annually (Tropeano, Spaggiari et al. 2019). As the leading cause of death and disability for individuals under 45 years of age (Xiong, Mahmood et al. 2013), understanding TBI's effects on brain function (e.g., connectivity) and evaluating the impact of various treatments are essential. Functional magnetic resonance imaging (fMRI) holds great potential for assessing alterations in brain functional connectivity post-TBI by tracking network recovery effects due to novel therapeutics(Sanchez-Carrion, Fernandez-Espejo et al. 2008, Chai, Abd Hamid et al. 2022).

The pig model has become popular for TBI and other neurological disease studies (e.g., stroke)(Kinder 2019, Simchick, Scheulin et al. 2021) as a translational large animal model with similar size and neuroanatomy(Kinder 2019) with human. Research using the pig TBI model has increased, as it is more likely to predict human outcomes and contribute to improved therapeutic devices and pharmacological treatment development. Our team recently demonstrated that pigs have homologous resting-state functional networks to human brains (Simchick, Shen et al. 2019) and identified functional connectivity disruptions due to TBI (Simchick, Scheulin et al. 2021), further emphasizing the pig model's importance for studying functional network changes.

Various methods have been applied to reveal functional connectivity, including model-free methods like sparse dictionary learning (sDL) (Mairal, Bach et al. 2009, Simchick, Shen et al. 2019, Simchick, Scheulin et al. 2021) and independent component analysis (ICA) (Smith, Jenkinson et al. 2004) , as well as seed-based methods (Cordes, Haughton et al. 2000) and functional connectome based cross-subject analysis (Amico and Goñi 2018, Benn, Mars et al. 2022). Since pigs require anesthesia during MRI scanning to reduce motion artifacts, task-based

fMRI meets many challenges. Existing resting-state fMRI (rs-fMRI) methods mostly use the spatial correlation between a known atlas and generated activation maps (Simchick, Scheulin et al. 2021) to evaluate recovery of brain functions after TBI while temporal correlation (e.g., the FSLNets (Smith, Jenkinson et al. 2004)) has been used for inter-network comparisons within a group. However, neither spatial nor temporal correlation analysis has employed a common baseline (e.g., a sham group in our porcine TBI study) for evaluating brain damages or disruptions of functional connectivity.

To evaluate TBI recovery and treatment effects, we introduced a novel method for cross-group correlation analysis, drawing inspiration from FSLNets' cross-group modeling and the broader framework of functional connectome studies, which has been proven important for individual fingerprinting(Finn, Shen et al. 2015). Our correlation studies assessed functional activity similarity between a TBI group and a sham group, where the sham group underwent only craniotomy surgery (Friess, Ichord et al. 2007), and the sham group's resting-state networks (RSNs) were considered to maintain normal functional connectivity. We extracted time series of RSNs from both TBI and sham groups' raw fMRI data using sDL or ICA for functional analyses. Those time series were then fed to FSLNets to investigate correlations between these groups, where a higher correlation with the sham group over two time points suggested improved brain function recovery compared to lower or unchanged correlations. We compared these temporal correlation findings with cerebral blood flow (CBF) maps derived from arterial spin labeling (ASL) data. Consistent with previous studies that demonstrated a strong spatial correlation between CBF maps and functional connectivity patterns, our analysis revealed that both the CBF spatial results and the temporal correlation trends exhibited similar patterns, reinforcing the validity of our findings in tracking recovery after TBI.

To better understand the TBI evaluation results, our study employs a simulation that mimics the progression of TBI from mild to severe by adding varying levels of Gaussian noise to experimental data in a larger pig dataset. This step was crucial for testing the sensitivity of our methods in detecting the nuances of recovery, ensuring our findings could offer significant insights into the dynamic processes of healing post TBI. Our results reveal distinct differences across the spectrum of injury severity, further validated by comparison with real DTI data.

This study contributes two major advancements compared to our previous research. First, it employs a temporal-spatial correlation analysis strategy for functional connectivity. Second, it uncovers functional changes in TBI groups by comparing network behaviors to a common baseline (i.e., a sham group) at two post-TBI timepoints.

Methods

Animal preparation and MRI data acquisition

A total of 18 castrated 4-week-old male crossbreed piglets were used in this study. They were randomly assigned to one of three groups: sham craniectomy + saline (n=6, referred to as Sham group), TBI + saline (n=6, referred to as SLN group), and TBI + fecal microbial transplant (FMT) (n=6, referred to as FMT group). FMT or saline were administered by oral gavage beginning 2-hours post-injury and then every 24 hours for 7 days. The moderate-severe TBI was conducted using our previously published procedure.(Baker, Kinder et al. 2019, Kinder, Baker et al. 2019, Kinder, Baker et al. 2019) Briefly, all pigs were anesthetized and underwent a 20mm craniectomy surgery at the left anterior junction of the coronal and sagittal sutures. Pigs were then secured in a controlled cortical impactor (CCI) device and a 15 mm impactor tip was positioned

over the intact dura to induce injury in the sensorimotor network region (Simchick, Scheulin et al. 2021) with the following parameters: velocity of 4m/s, depth of depression of 9mm, and dwell time of 400ms. All experimental procedures were approved by the Institutional Animal Use and Care Committee (IAUCC) at the University of Georgia.

MRI was conducted on all pigs at two timepoints, day 1 (D1) and day 7 (D7) post-surgery. Pigs were anesthetized and mild anesthesia was maintained via inhalation isoflurane for the duration of the scans. T1-weighted anatomical, rs-fMRI, and ASL data were collected using a GE 32-channel fixed-site Discovery MR750 3.0 Tesla magnet and an 8-channel knee coil. T1-weighted anatomical, rs-fMRI, and ASL data were acquired using the following sequences: (1) 3D fast spoiled gradient echo (FSPGR) sequence (repetition time TR=5.5s, echo time TE=2.1ms, flip angle FA=9°, field-of-view FOV=12.8x12.8x6.4cm, slice thickness=1mm, a reconstruction matrix size of 256x256x112 (resulting in cubic voxels of 0.5 mm), axial slice plane, and an acquisition time of 10min57s, and (2) gradient echo-planar imaging (EPI) sequence (TR=3s, TE=30ms, FA=80°, FOV=12.8x12.8x6.2 cm, a matrix size of 96x96x31, coronal slice plane, 305 total volumes for rs-fMRI an acquisition time of 15min15s. (3) 3D pseudo-continuous ASL sequence (FOV=12.8 cm x 12.8 cm, slice thickness 3mm, frequency/phase encoding of 512 and 8).

Data preprocessing and RSN node selection

First, all rs-fMRI and ASL images were registered to a reference space using statistical parametric mapping (SPM12) in MATLAB 2021b. A whole-brain masking was performed for each subject to isolate the brain from surrounding tissues, and the brain was subsequently registered to the T1-weighted images in the anatomical space.

In this study, two machine learning models, ICA (FSL MELODIC(Smith, Jenkinson et al. 2004)) and sDL(Kreutz-Delgado, Murray et al. 2003), were applied for temporal analysis, aiming to reveal effect of recovery from TBI. We divided the data into two distinct datasets for machine learning analysis: the Full Dataset Learning (FL), containing rs-MRI dataset of both TBI and sham groups (Sham+SLN+FMT), and the Sham Dataset Learning (SL), which includes only dataset of the sham group (Sham). The FL dataset, featuring a broader subject set, was intended to capture a comprehensive representation of recovery process covering both TBI and craniectomy. In contrast, the SL dataset focused on establishing a baseline with standard features from the sham group (craniectomy) alone. Applying either ICA or sDL to either FL or SL datasets led to four experimental conditions, thereby facilitating a thorough assessment of result consistency across these varied scenarios.

For each experimental condition, ICA was employed to identify 100 group-level independent components, and sDL was used to detect 300 atoms, with both independent components and atoms representing distinctive patterns of brain functions. These identified components and atoms were then projected back to co-registered, template pig brain's T1-images for mapping of various brain functions, thresholded by a z-score of 1, smoothed, and correlated with seven predefined atlases of resting-state networks (RSNs, as elaborated in Table 2.1). The component or atom exhibiting the highest Pearson correlation with any of the seven RSNs was chosen as its corresponding representative RSN node. Leveraging the FSL dual regression technique, we extracted the time series for each subject corresponding to the seven RSN nodes. These time series were then analyzed to construct functional connectivity matrices, offering insights into brain functional connectivity patterns.

Cross-group Temporal Correlation analysis

Since the focus of this study is the evaluation of post-TBI brain function recovery, a baseline is necessary for cross-group evaluations. As the sham group pigs received only the craniectomy surgery and saline, their RSNs are assumed to maintain normal functional activities, accompanied by the craniectomy effect at different time points (D1 and D7). This hypothesis enables us to use the sham group based RSNs as the baseline for brain function recovery evaluation of TBI groups.

Our analysis involved a multi-step process. We combined time series data from matching nodes of TBI (SLN or FMT) and control (Sham) subjects to create a pseudo subject to effectively calculate correlation matrices and assess connectivity changes for the same node cross group (details in APPENDIX A).

To mitigate potential biases from the sequence of concatenation and account for variability in recovery status among the TBI-treated pigs, we introduced a shuffling mechanism with multiple trials and a drop-one-out strategy. Specifically, in each iteration, one subject was randomly excluded, and the remaining subjects were shuffled before recombination. This procedure was repeated 128 times, ensuring robustness against bias and variability from individual differences and outlier effects.

Simulation

In order to underscore the efficacy of our cross-group temporal correlation analysis, we undertook a simulation study leveraging rs-fMRI data from 44 healthy piglets, matched in age to our study subjects and collected using identical rs-fMRI protocols(Fang, Sun et al. 2020). Utilizing

the same seven RSN nodes (detailed in Table 2.1), we generated time series for each node via the dual-regression procedure outlined earlier. These time series were normalized to have zero mean and a standard deviation of one.

To mimic disrupted functional activities indicative of TBI, we introduced Gaussian noise at varying intensities to the time series of three specific networks (EXN, SMN, and DMN). This created two simulated TBI groups to represent mild and severe injury levels, respectively. The entire dataset of 44 was then categorized into three: a control (sham) group of 14 subjects without added noise, simulating normal brain function; a simulated mild TBI group of 14 subjects with low-level noise (standard deviation of 1); and a simulated severe TBI group of 16 subjects with high-level noise (standard deviations of 3, 5, 7, 10, and 15) to represent varying degrees of injury severity.

We conducted temporal correlation analyses between the sham group and each of the simulated TBI groups to validate our method's statistical robustness in distinguishing between different levels of brain injuries.

Spatial Correlation Analysis

In addition to the temporal correlation analysis using rs-fMRI, we also performed a spatial correlation analysis by obtaining cerebral blood flow (CBF) maps associated with the seven resting-state networks (RSNs) using acquired ASL data. We masked the whole brain CBF map for each subject with the seven RSNs. For each RSN, we employed a similar methodology to the temporal correlation of rs-fMRI data for CBF spatial correlations (details in APPENDIX A).

Results

Pigs with TBI injuries showed significant brain lesioning and edema at D1 and D7 relative to sham pigs (Figure 2.1). The pathophysiology of TBI pigs were consistent with moderate-severe TBI as previously reported by our research group (Kinder, Baker et al. 2019, Kinder, Baker et al. 2019).

Simulation Assessment

The simulation results are displayed in Figure 2.2. The gray bars represent similarities between the simulated sham group and the simulated mild TBI group, while the black bars indicate similarities between the simulated sham group and the simulated severe TBI group at various noise levels (standard deviation of 1, 3, 5, 7, 10, and 15, respectively). The difference between the gray and black bars consistently grows with the noise level in the severe TBI group across all three networks. This difference reaches statistical significance at noise level 15 for the EXN, and 7 for the DMN in the severe TBI group.

Temporal Correlation Analysis

The temporal correlation results for the TBI groups versus the sham group from D1 to D7, obtained by ICA and sDL analysis, are displayed in Figure 2.3 A) and B), respectively. The results represent the similarities between the sham group and the TBI group at D1 using blue bars and at D7 using red bars.

For the SLN treated group, the SMN showed a significant decrease in the ICA result (Figure 2.3A). Five out of seven RSNs displayed decreased correlations in both the full-dataset learning (FL) and the sham-dataset learning (SL) results, with SMN, AUD, and BAS being

consistent. Meanwhile, no consistent increasing trends between FL and SL were identified in any other RSNs. In the sDL analysis of temporal analysis (Figure 2.3B), the VIS, AUD, and BAS networks exhibited significant decreases in the SL results, while the remaining four RSNs showed a decreasing trend in the SL results.

For the FMT treated group, the EXN and SAL showed significant increases in FL results, while the EXN, SMN, and AUD networks had consistent increasing trends in both FL and SL results. No consistent decreasing trends between FL and SL were observed. In the sDL analysis, the SAL network displayed a consistent, significant increase in both FL and SL results, while the EXN showed a consistently increasing trend between FL and SL results.

Overall, the temporal analysis indicates that the FMT group exhibits a consistent increase in the EXN network, while the SMN and SAL networks show three instances of increases and one decrease. No network had more than two instances of decrease. All three increases of the SAL in the FMT group were statistically significant. For the SLN group, the SMN network demonstrated consistent decreases across all four trials (ICA/sDL both with FL/SL), while the EXN, AUD, DMN, and BAS networks displayed three instances of decreases but one instance of increase. No network had more than two instances (half of the trials) of increases in the SLN group. The visualization of activation maps corresponding to two of the temporally changed nodes (EXN, SAL) is shown in Figure 2.4, providing an approximate impression of those nodes and associated changes.

Spatial Correlation Analysis

The results of the spatial correlation analysis are presented in Figure 2.5. The top and bottom rows depict CBF spatial correlations for the seven RSNs in the SLN and FMT groups

compared to the sham group, respectively. The lower part of Figure 2.4 presents visualized CBF maps for the EXN and SAL networks, providing an approximate impression of the spatial distribution and changes in these networks' CBF correlations.

For the SLN group, no significant increases or decreases in CBF correlations were observed, suggesting that the SLN group without treatment did not lead to noticeable changes in CBF spatial correlations within the RSNs.

In contrast, the FMT group showed significant increases in correlation strength for the EXN and SAL networks from D1 to D7. This finding is consistent with the trends observed in the temporal correlation analysis (Figure 2.3) for the same two RSNs, indicating that the FMT treatment may have a positive impact on the spatial correlation of CBF within these networks.

Discussion and conclusion

In our study, we assessed brain function recovery in a pig TBI model using temporal and spatial correlations. The findings indicate that FMT treatment resulted in enhanced recovery compared to the SLN group, as shown by increased functional connectivity correlations with the sham group from D1 to D7. Notably, consistent trends of improvement were observed in the EXN and SAL RSNs for the FMT group, with significant increases in both temporal and spatial correlations indicating potential recovery. Specifically, the SAL RSN showed significant temporal increases in three out of four trials and a notable spatial correlation increase, while the EXN RSN, despite not reaching statistical significance, displayed consistent upward trends in temporal analysis and a significant spatial improvement.

Conversely, the SLN group exhibited consistent declines in functional indicators across the SMN, AUD, and DMN networks, suggesting worsening conditions post-TBI. These contrasting

trends underscore the potential of FMT treatment in facilitating recovery and highlight the critical role of monitoring specific RSNs in evaluating TBI treatment efficacy.

Furthermore, the simulation results showed consistent decrease in correlation (Figure. 2.3) with TBI progression as the noise intensity increases (in the simulation of TBI severity). While the incorporation of Gaussian noise serves as a rudimentary approximation of TBI—given that actual injuries can introduce more complex noise patterns—our results remained consistent. This consistency indicates the effectiveness of the cross-group methodology in evaluating brain function recovery across all three RSNs. Additionally, the similarity between the simulated mild group and the sham group also proved the stability of the cross-group temporal correlation methodology. These results demonstrate that the cross-group correlation study is a stable and reliable method for evaluating brain function recovery. The cross-group correlation could potentially have practical applications in clinical settings for assessing the effectiveness of TBI treatment strategies.

In this study, we identified the most relevant ICA components and SDL atoms based on their Pearson correlation with each of the seven RSNs and defined them as nodes (see Supplementary Figure A2). The components/atoms were learned by group-level ICA and sDL approaches, with either FL or SL dataset on D1 and D7 together. Both ICA and sDL approaches decompose the group dataset into combinations of matrices (component matrix, atoms/dictionary matrix, and their corresponding coefficient matrix), yet they reveal distinct features due to their underlying principles. ICA tends to isolate more distinct and focused components, aligning with its goal to uncover independent signals within the data. Conversely, SDL often produces broader, more inclusive results, capturing larger activation areas that may encompass multiple features,

thereby showing adaptability to smaller datasets. This contrast makes them complementary tools in our study and offers a multifaceted understanding of the recovery effect, allowing us to gain a comprehensive insight into brain function recovery post-TBI.

Utilizing the sham group as a baseline for brain function comparison allowed the RSN nodes to represent normal brain functions, acknowledging that the sham group, reflecting the craniectomy's effects, provides a more accurate baseline than a healthy control group. Nonetheless, the study faces limitations, notably the small size of the sham group (6 subjects), limiting the effectiveness of deep learning approaches. Additionally, the dual regression procedure's reliance on the sham dataset for defining nodes might introduce errors due to anatomical variations between TBI and sham subjects, potentially leading to inaccurate time series and activation maps. Conversely, learning from the full dataset (FL), which contains both sham and TBI groups, might highlight TBI-associated activities as fault 'features' diverging from the objective of identifying nodes indicative of normal functions. This inclusion of TBI subjects introduces further uncertainty in distinguishing between normal and recovery-related brain functions, making it challenging to determine which dataset, SL or FL, more accurately represents recovery effects. Our findings did not definitively show that one dataset outperforms the other in characterizing brain function recovery. Acknowledging these challenges is crucial for interpreting the results and guiding future research. Future efforts should focus on increasing sample sizes, refining learning methods, or exploring new approaches to accurately represent normal brain functions.

It is noted that negative correlation coefficients existed in the raw correlation matrices obtained from temporal correlation analysis. While positive correlation coefficients were considered to represent the similarity of the comparing components, negative correlation

coefficients were ambiguous. Some studies (Chen, Chen et al. 2011) suggest these negative values represent negative correlation in which one component increases as the other component decreases. Although some assumptions have been made in studies connecting the negative values with structural or functional connectivity in the brain (Schwarz and McGonigle 2011), there are no straightforward built-in relationships between negative correlation effects and functional connectivity. We adopt the same methodology as previous studies by rejecting negative functional connectivity results to avoid uncertainty (Buckner, Sepulcre et al. 2009, Meunier, Achard et al. 2009). However, it is essential to acknowledge the limitations of this approach and consider discussing the potential implications of negative correlation coefficients in future research. Exploring alternative methods for handling negative correlation coefficients or investigating whether they could provide additional insights into the functional connectivity of the brain may be valuable directions for future studies.

In this study, we reported increased correlations in only two out of a total of seven RSNs in pig brains post-TBI. However, because the evaluations were made only six days apart, it is possible that some RSNs may not have had adequate time to show significant changes. The high level of variability is possibly due to injury, and more robust changes may be seen with decreased variability in the later stage of recovering brains. Future studies may consider a longer period of recovery time for a thorough evaluation of functional activities and explore how these findings could be applied to other neurological disorders.

In summary, our study focused on evaluating post-TBI recovery, revealing the effectiveness of FMT treatment through the innovative use of temporal correlation analysis of rs-fMRI data alongside spatial correlation of CBF maps from ASL data. This temporal-spatial cross-

group correlation approach not only confirmed the consistency of functional recoveries within resting-state networks (RSNs) across both simulated and experimental datasets, but also underscored the utility of this novel method in accurately assessing functional activity changes following TBI and other neurological disorders. By offering a detailed insight into the recovery processes post-TBI, this method stands to significantly impact neuroscience, providing a robust framework for evaluating the outcomes of neural treatments.

Acknowledgement

The authors would like to thank Savannah Cheek, Ethan Karstedt, and Kim Mason for assistance with MRI acquisition, as well as our team of undergraduate researchers.

Author Contribution

W.S.: Primary author of the article, contributed to the development of the methodology, data analysis and interpretation, and drafted the major portion of the article. W.R.: contributed to data analysis and article revision. M.M.F.: contributed to concept and design of the study, conducted the experiment, and article revision. C.B.W., K.M.S., S.E.S., T.R.C., and K.J.D.: contributed to the design of experiment, and conducted the experiment. F.D.W. and Q.Z.: contributed to concept and design of the study, the development of the methodology, data interpretation, and article revision.

Author Disclosure Statement

All authors have nothing to disclose for the purpose of this study.

Funding Information

This work was supported by the National Institutes of Health grant number R21NS119167 and the University of Georgia Innovative and Interdisciplinary Research Grant.

Transparency, Rigor and Reproducibility Summary

The study was registered following the example of previous studies by 'Simchick, G., et al. (2021). "Detecting functional connectivity disruptions in a translational pediatric traumatic brain injury porcine model using resting-state and task-based fMRI." Scientific reports 11(1): 1-19'[1]. The analysis plan was likewise registered in accordance with this precedent[2]. Eighteen (n=18) pigs were involved in the study and data was collected at two timepoints, i.e., 1- and 7-day post TBI[6]. A simulation was conducted using an additional 44 pigs as well.. All eighteen pigs were included in the data analysis[4]. No special equipment or software was used in process[7]. The key inclusion criteria (e.g., primary diagnosis or prognostic factor) are established standards in field[8]. Implications of possible violations of these assumptions include normal distribution of data and normal functional activities in Sham group[9]. Methods that do not require correction for multiple comparisons were used, including anova[10]. At the time of writing, a replication study has not yet been planned[11]. De-identified data from this study, along with the analytic code used to conduct the analyses, will soon be publicly available on GitHub[12,13]. This paper will be published under a Creative Commons Open Access license, and upon publication, will be freely available at https://www.liebertpub.com/loi/neu[14].

References

1. Tropeano MP, Spaggiari R, Ileyassoff H, et al. A comparison of publication to TBI burden ratio of low- and middle-income countries versus high-income countries: how can we improve worldwide care of TBI? Neurosurg Focus 2019;47(5):E5, doi:10.3171/2019.8.FOCUS19507

2. Xiong Y, Mahmood A, Chopp M. Animal models of traumatic brain injury. Nat Rev Neurosci 2013;14(2):128-42, doi:10.1038/nrn3407

3. Sanchez-Carrion R, Fernandez-Espejo D, Junque C, et al. A longitudinal fMRI study of working memory in severe TBI patients with diffuse axonal injury. Neuroimage 2008;43(3):421-9, doi:10.1016/j.neuroimage.2008.08.003

4. Chai WJ, Abd Hamid AI, Omar H, et al. Neural alterations in working memory of mild-moderate TBI: An fMRI study in Malaysia. J Neurosci Res 2022, doi:10.1002/jnr.25023

5. Simchick G, Scheulin KM, Sun W, et al. Detecting functional connectivity disruptions in a translational pediatric traumatic brain injury porcine model using resting-state and task-based fMRI. Sci Rep 2021;11(1):12406, doi:10.1038/s41598-021-91853-5

6. Kinder HA, E. W. Baker and F. D. West. The pig as a preclinical traumatic brain injury model: current models, functional outcome measures, and translational detection strategies. Neural regeneration research 14(3): 413 2019;

7. Simchick G, Shen A, Campbell B, et al. Pig Brains Have Homologous Resting State Networks with Human Brains. Brain connectivity 2019;ja):

8. Mairal J, Bach F, Ponce J, et al. Online dictionary learning for sparse coding. 2009.

9. Smith SM, Jenkinson M, Woolrich MW, et al. Advances in functional and structural MR image analysis and implementation as FSL. Neuroimage 2004;23 Suppl 1(S208-19, doi:10.1016/j.neuroimage.2004.07.051

10. Cordes D, Haughton VM, Arfanakis K, et al. Mapping functionally related regions of brain with functional connectivity MR imaging. AJNR Am J Neuroradiol 2000;21(9):1636-44

11. Benn RA, Mars RB, Xu T, et al. Opening the Pig to Comparative Neuroimaging: A Common Space Approach Contextualizes the Pig and Human Structural Connectome. bioRxiv 2022;2020.10.13.337436, doi:10.1101/2020.10.13.337436

12. Amico E, Goñi J. The quest for identifiability in human functional connectomes. Scientific reports 2018;8(1):1-14

13. Finn ES, Shen X, Scheinost D, et al. Functional connectome fingerprinting: identifying individuals using patterns of brain connectivity. Nat Neurosci 2015;18(11):1664-71, doi:10.1038/nn.4135

14. Friess SH, Ichord RN, Owens K, et al. Neurobehavioral functional deficits following closed head injury in the neonatal pig. Experimental neurology 2007;204(1):234-243

15. Baker EW, Kinder HA, Hutcheson JM, et al. Controlled Cortical Impact Severity Results in Graded Cellular, Tissue, and Functional Responses in a Piglet Traumatic Brain Injury Model. J Neurotrauma 2019;36(1):61-73, doi:10.1089/neu.2017.5551

16. Kinder HA, Baker EW, Howerth EW, et al. Controlled cortical impact leads to cognitive and motor function deficits that correspond to cellular pathology in a piglet traumatic brain injury model. Journal of Neurotrauma 2019;36(19):2810-2826

17. Kinder HA, Baker EW, Wang S, et al. Traumatic brain injury results in dynamic brain structure changes leading to acute and chronic motor function deficits in a pediatric piglet model. Journal of Neurotrauma 2019;36(20):2930-2942

18. Kreutz-Delgado K, Murray JF, Rao BD, et al. Dictionary learning algorithms for sparse representation. Neural computation 2003;15(2):349-396

19. Fang X, Sun W, Jeon J, et al. Perinatal docosahexaenoic acid supplementation improves cognition and alters brain functional organization in piglets. Nutrients 2020;12(7):2090

20. Chen G, Chen G, Xie C, et al. Negative functional connectivity and its dependence on the shortest path length of positive network in the resting-state human brain. Brain connectivity 2011;1(3):195-206

21. Schwarz AJ, McGonigle J. Negative edges and soft thresholding in complex network analysis of resting state functional connectivity data. Neuroimage 2011;55(3):1132-1146

22. Buckner RL, Sepulcre J, Talukdar T, et al. Cortical hubs revealed by intrinsic functional connectivity: mapping, assessment of stability, and relation to Alzheimer's disease. Journal of neuroscience 2009;29(6):1860-1873

23. Meunier D, Achard S, Morcom A, et al. Age-related changes in modular organization of human brain functional networks. Neuroimage 2009;44(3):715-723

Resting-state network	Anatomies associated with each RSN
Executive Control Network (EXN)	Primary Somatosensory Cortex Dorsolateral Prefrontal Cortex Anterior Prefrontal Cortex Orbitofrontal Cortex Insular Cortex Ventral anterior Cingulate cortex Dorsal Anterior Cingulate Cortex
Visual Network (VIS)	Primary Visual Cortex Secondary Visual cortex Associative Visual cortex
Sensorimotor Network (SMN)	Primary Motor Cortex Somatosensory Association Cortex Premotor Cortex
Auditory Network (AUD)	Superior Temporal Gyrus Auditory Cortex
Default Network (DMN)	Hippocampus Anterior Prefrontal Cortex Inferior Temporal Gyrus Ventral Posterior Cingulate Cortex Retrosplenial Cingular Cortex Dorsal Posterior Cingular Cortex Anterior Entorhinal Cortex Parahippocampal Cortex
Salient Network (SAL)	Caudate Nucleus Globus Pallidus Insular Cortex Middle Temporal Gyrus Ventral Posterior Cingulate Cortex Ventral Anterior Cingulate Cortex Retrosplential Cingular cortex Dorsal Posterior Cingular Cortex Dorsal anterior Cingulate Cortex
Basal Ganglia Network (BAS)	Anteroventral Thalamic Nucleus Central Thalamic Area Mediodorsal Thalamic Nucleus Laterodorsal Thalamic Nucleus Reticular Thalamic Nucleus Ventral Anterior Thalamic Nucleus Ventral Posterior Thalamic Nucleus Caudate Nucleus Globus Pallidus Amygdala Primary Motor Cortex Orbitofrontal Cortex Parahippocampal Cortex

Table 2.1. Seven RSNs and their associated anatomies.

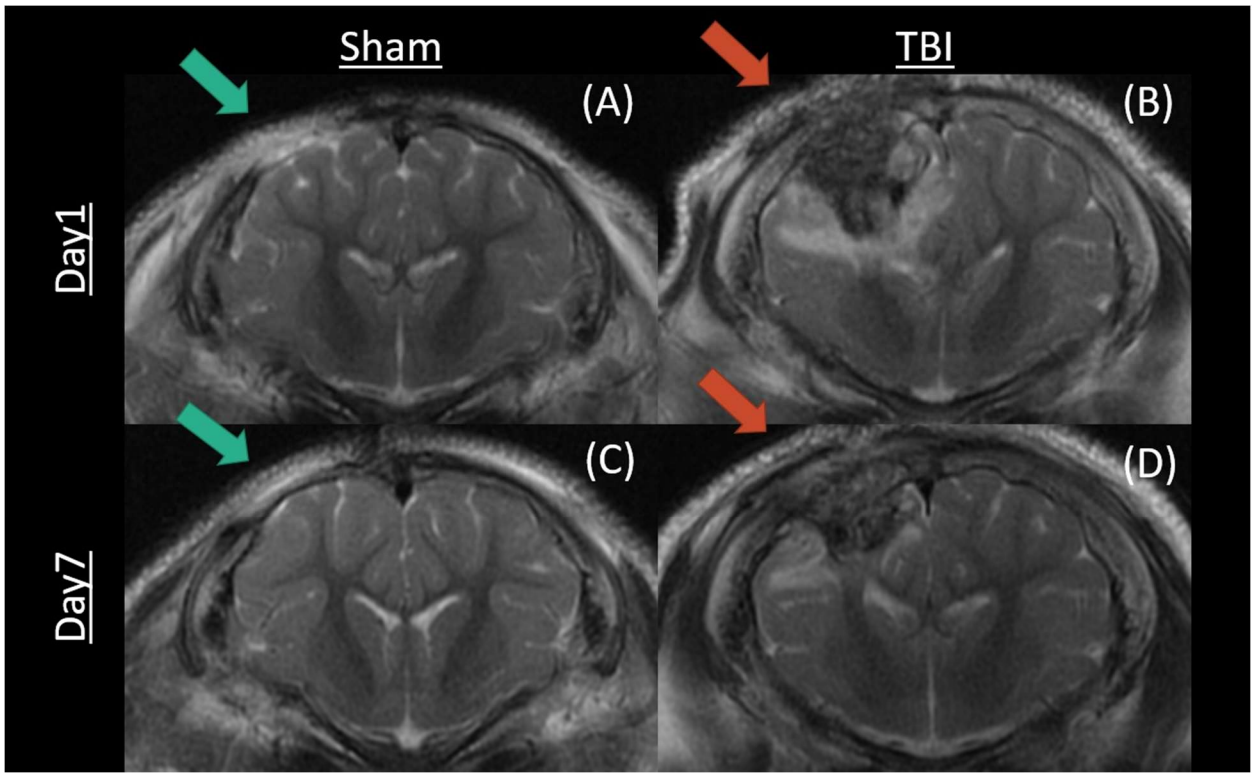

Figure 2.1: Representative visualizations of sham and TBI pigs. Left column: sham pig; right column: TBI pig; top row: day 1 images; bottom row: day 7 images. Blue arrows indicate the craniectomy surgical site, while red arrows point to the TBI injury.

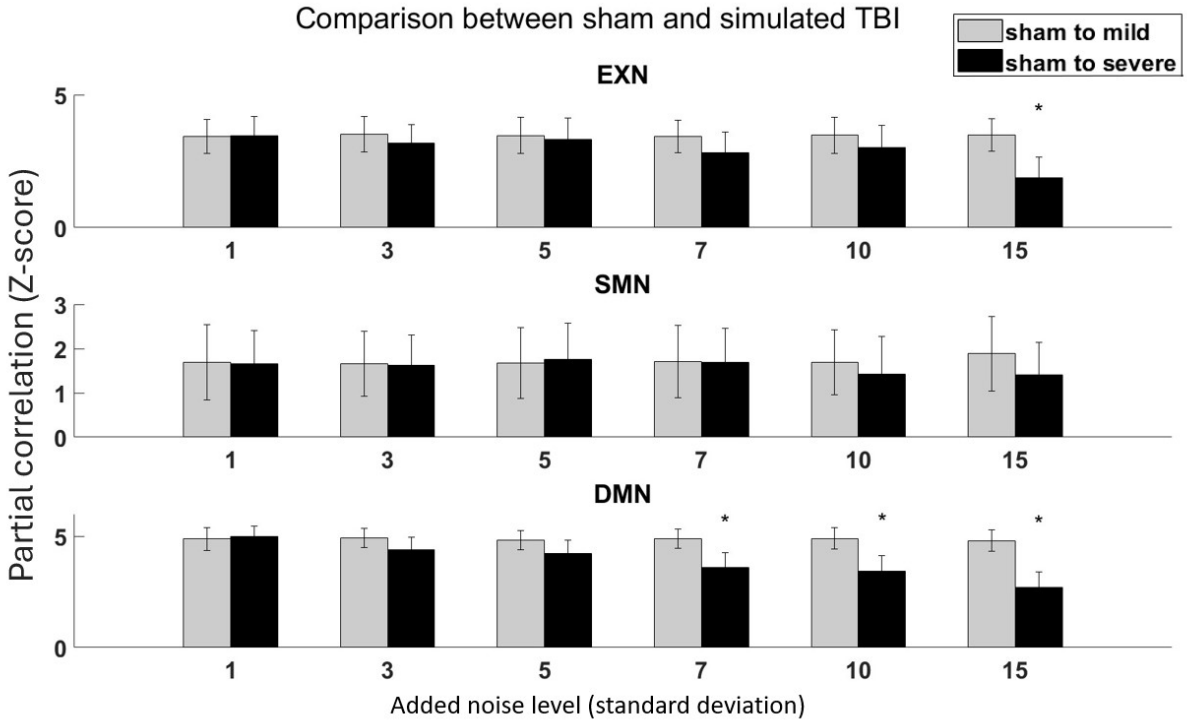

Figure 2.2: Simulation results of correlations between the sham to simulated mild and sham to simulated severe TBI injuries. Gray bars represent comparisons of sham to simulated mild TBI group. Black bars represent comparisons of sham to simulated severe TBI group at the added noise levels of standard deviations of 1, 3, 5, 7, 10, and 15 for each of the RSN nodes. Generally, stable trends are observed for the gray bars, while descending trends are observed for the black bars in all three RSNs. These results indicate that similarities between the sham and TBI groups decreased with increasing simulated TBI severity. Star signs indicate statistically significant differences.

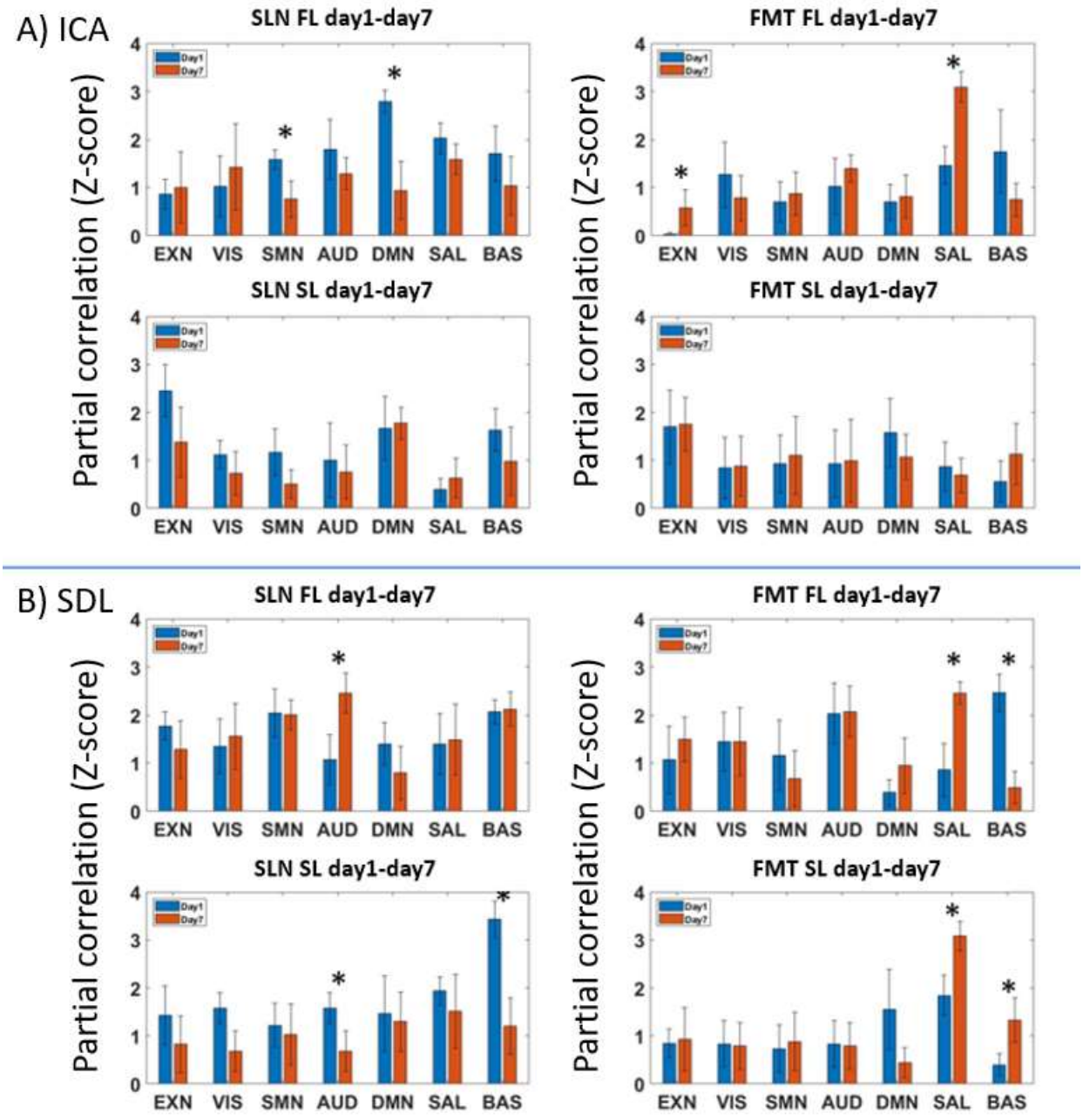

Figure 2.3: Temporal analysis results using A) ICA and B) sDL approaches. In each section, the first row shows full dataset learning (FL) results, and the second row displays sham dataset learning (SL) results. The left side represents the SLN group, and the right side represents the FMT group. Similarities between the sham group and the TBI group at day 1 are presented by

blue bars, and at day 7 by red bars. The x-axis shows the 7 RSN nodes, while y-axis shows Fisher transformed partial correlations as Z-stats. Results are reported as means with error bars. Star signs indicate statistically significant differences with a p-value <0.05.

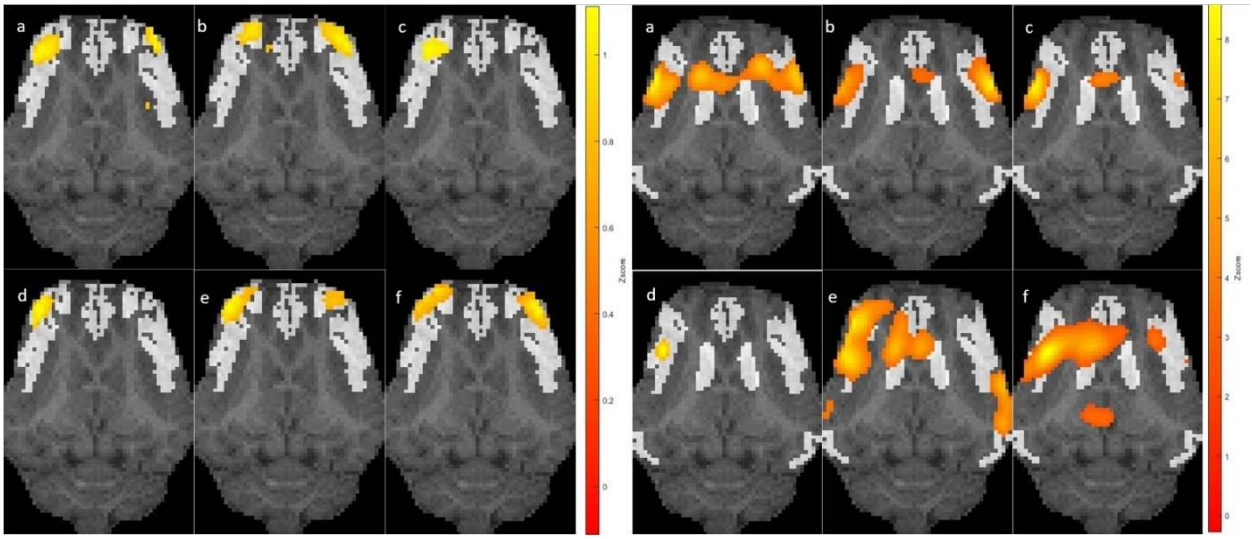

Figure 2.4: Representative activation maps for two RSNs, EXN (executive control network, left) and SAL (salience network, right). Each subfigure displays (a) an SLN group pig, (b) a sham group pig, and (c) an FMT group pig at day 1 (top row), (d) an SLN group pig, (e) a sham group pig, and (f) an FMT group pig at day 7 (bottom row). All correlation maps (color) are overlaid on a registered template pig anatomical image (gray). Sections overlaid on anatomical images are registered to an atlas for each RSN.

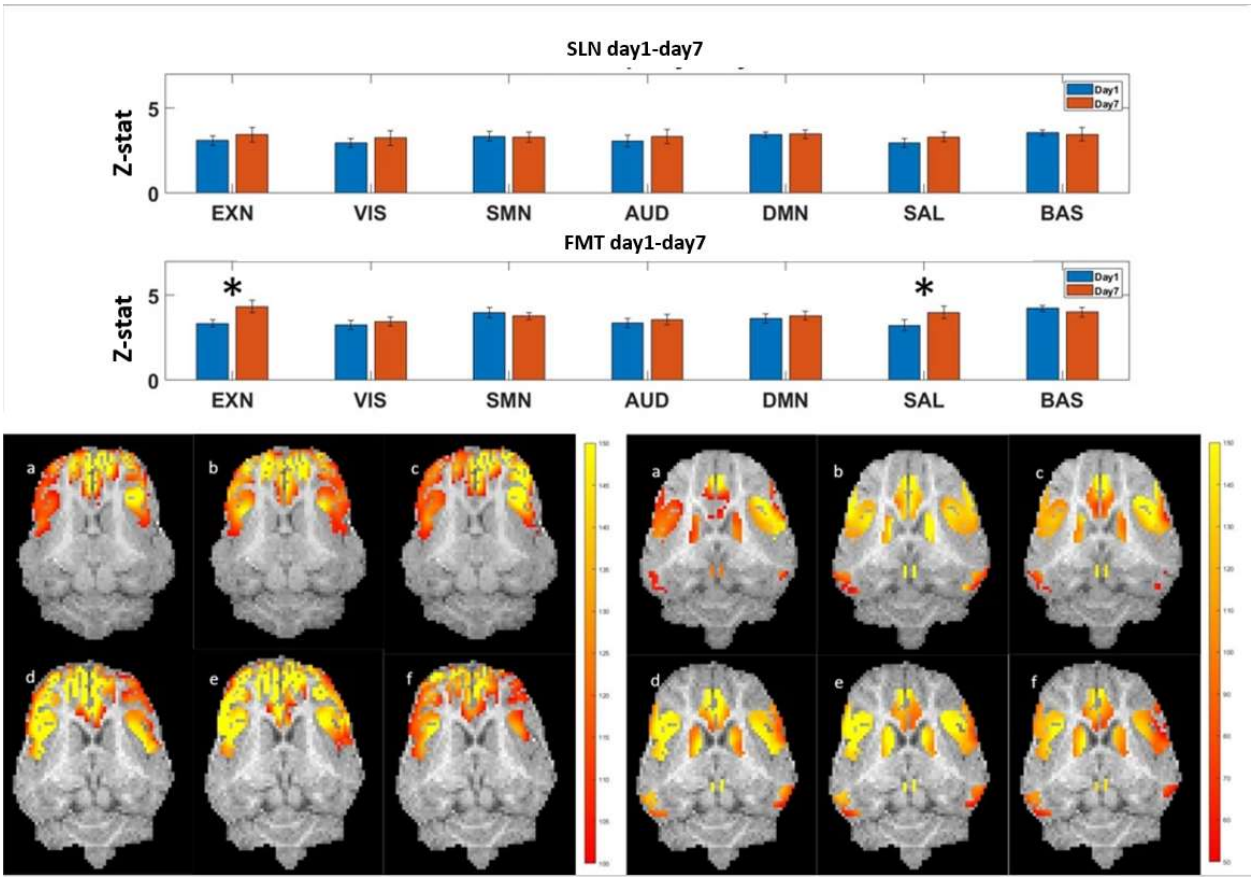

Figure 2.5: Spatial CBF correlation analysis for SLN (top bar plot) and FMT (bottom bar plot) groups, and representative spatial CBF maps for two RSNs, EXN (left) and SAL (right). In the top graph, similarities between the sham group and the TBI groups at day 1 and day 7 are shown by the blue and red bars, respectively. Results are reported as means with error bars. Star signs indicate statistically significant differences with a p-value < 0.05. In the bottom visualization graph, each sub-figure shows (a) an SLN group pig, (b) a sham group pig, and (c) an FMT group pig at day 1 (top row), (d) an SLN group pig, (e) a sham group pig, and (f) an FMT group pig at day 7 (bottom row). All CBF maps (color) are overlaid on a registered template pig anatomical image (gray).

CHAPTER 3

AFFINITY OF STRUCTURAL WHITE MATTER TRACTS BETWEEN INFANT AND ADULT PIG[2]

[2] Sun, W., Ahmed, I., Dubrof, S., Park, H.J., West, F., and Zhao, Q. Accepted by *Journal of Neuroscience Methods.* Reprinted here with permission of the publisher, April 2024.

Abstract

Background

The piglet brain has been increasingly used as an excellent surrogate for investigation of pediatric neurodevelopment, nutrition, and traumatic brain injuries. This study intends to establish a piglet brain's structural connectivity model and compare it with the adult pig, enhancing its application for structurally guided functional analysis.

Methods

In this study, diffusion-weighted (DW)-MRI data from piglets (n=11, 3-week-old) was used to establish piglet model and compare with adult pigs. We employed a data-driven independent component analysis (ICA) method to derive piglet-specific tracts. Pearson correlations and Kullback-Leibler (KL) divergences was employed to identify common tracts and unique tracts for piglet. Common tracts were then used in a blueprint connectome study to highlight differences in regions of interest (ROI).

Results

The data-driven approach applied to piglet brains revealed 17 common tracts, showing high similarity with adult pigs' white matter (WM) tracts, and identified 3 tracts unique to piglets and 10 negative marker tracts. Additionally, the study highlighted notable differences in 3 ROIs associated with blueprint connectome.

Comparing with existing methods

This study marks a significant shift from surface-based to voxel-based methodologies in analyzing pig brain structural connectivity and generating connectome blueprints. Additionally, it sheds light on the use of the piglet model for developmental studies, offering new perspectives in this area.

Conclusion

This study established a piglet brain tract model and conducts a comparative analysis of adult pig's and piglet's structural connectivity. These findings underscore the potential use of the piglet brain model in employing piglet model for developmental studies.

Introduction

Animal models have long been an essential tool in neuroscience research, served as translational models for human brains[1,2]. There has been a growing interest in using the pig model for such purposes[3-5]. The pig is an effective translational model in many ways, including the fact that both the pig and human brain are composed of more than 60% white matter [6-9]. Humans and pigs both have gyrencephalic brains, a key architectural difference directly correlated with brain connectivity and complexity [6-8].

The adult pig brain has recently been structurally mapped and shown to share a common connectivity space with the human brain, facilitating pig-human cortical alignment[10]. Meanwhile, a piglet model has also demonstrated great potentials to be a pediatric surrogate model for long-term recovery after brain injury[11,12], neurodevelopment, and nutritional supplements [13,14]. Yet, research on infant pig brain structural connectivity is limited.

In this study, our main goal is to create a detailed map of the connections in piglet brains, focusing on identifying the pathways (white matter tracts) that are similar between young piglets and adult pigs. We also aim to compare these tracts and regions of interest in piglets with those in adult pigs to understand how they are structured and interconnected. We acquired Diffusion-Weighted Magnetic Resonance Imaging (DW-MRI) data from healthy piglets and employed independent component analysis (ICA) to the structural connectivity matrices to identify white matter tracts. This data-driven approach is rooted in earlier studies that explored cortical surface-based structural connectivity in adult pig and human brains[10,15-17]. Our study diverges by adopting

a voxel-based methodology, utilizing gray matter masks to generate data-driven tracts (DDT). Additionally, we employed structural connectome blueprints in our study, a concept introduced by Mars, Sotiropoulos et al. [18]. These blueprints provide profound insights into the complex structural connectivity among various brain regions of interest (ROIs), including both cortical structures and key white matter structures. By converting structural connections into feature vectors, our approach enables direct comparisons between different brains at a consistent dimensional scale (number of ROIs times number of tracts).

Our findings reveal 17 tracts within the piglet brain that closely resemble the adult pig's white matter atlas tract (WMAT), underscoring significant structural similarities. Notably, our analysis also uncovers 3 unique tracts in piglets, offering novel insights into the structural nuances of the piglet model. The identified 17 common white matter tracts are employed, together with 26 symmetrical pairs of ROIs, a total of 52 ROIs consisting of major cortical structures, to generate structural connectivity blueprints. These ROIs, sourced from Saikali's anatomical atlas[19], keep sizes that are suitably robust for transformation between adult and piglet brains. Utilizing Kullback-Leibler (KL) divergence [20], we conduct a comparative analysis of the connectome properties of each major ROI between adult and piglet brains. Details of employed ROIs can be found in APPENDIX B

The proposed structural connectivity model is expected to extend beyond this study's scope; it will likely have far-reaching effects for future research in neuroscience. Using pigs as a translational, large animal model for research can provide deep insights, especially when looking at how the brain changes and develops over time. Our study sheds light on these changes and paves the way for new areas of research, opening possibilities for more discoveries about the pig brain.

Methods

Animal preparation and MRI data acquisition

In this study, T1-weighted anatomical and diffusion-weighted (DW)-MRI data were obtained from a group of healthy, 3-week-old piglets (Landrace pigs, n = 11, 5 males and 6 females). The T1 and DW-MRI imaging data was collected using a GE 32-channel fixed-site Discovery MR750 3.0 Tesla magnet and an 8-channel knee coil using the following sequence and parameter. T1-weighted anatomical: 3D fast spoiled gradient echo (FSPGR) sequence (TR=5.5s, TE=2.1ms, FA=9°, FOV=12.8x12.8x6.4cm, slice thickness=1mm, and a matrix size of 256x256x112); DW-MRI: spin echo EPI sequence (TR=15.5s, TE=min-full, FOV=12.8x12.8x6.4cm, a matrix size of 64×64x32, 3 b=0 images, and 30 diffusion weighted images using b=1000s/mm2). All experimental procedures, including animal facility conditions and animal welfare, were approved and conducted in accordance with guidelines established by the University of Georgia Institutional Animal Care and Use Committee (IACUC, AUP# is A2021 01-026). The processed connectivity data for adult pigs (n=6) was obtained from a previously published study[10].

Data preprocessing and tract generation

The collected DW-MRI images were initially processed by skull stripping using the FSL Brain Extraction Tool (FSL bet[21]). Subsequently, corrections for Eddy current and motion artifacts were applied using FSL Eddy tool [22]. Additionally, image distortions caused by susceptibility were corrected also by using FSL Eddy tool, utilizing field maps generated by acquired phase images (FSL Prelude tool). The corrected DW-MRI images were subsequently provided as input to the

FSL BedpostX[23] procedure to generate voxel-based maps for probabilistic data-driven tractography analysis utilizing a two-fiber tensor model estimation.

To generate data-driven tracts, the methodology outlined in Figure 3.1A was implemented. Specifically, a gray matter (GM) voxel-based mask was generated using 139 out of 178 anatomies associated with GM from a pig brain atlas [19] and registered to each subject individually using Flirt[24]. With FSL Probabilistic Tractography (FSL probtractx[25]) software, virtual streamlines were initiated from each voxel in the GM mask and followed the tensor estimation obtained by FSL BedpostX to expand throughout the brain. The number of streamlines, out of a total of 5000 trials, that start at every possible voxel u in the GM mask and pass through every possible voxel v in the whole brain mask, was recorded as D_{uv}, which marks the probabilistic structural connectivity between voxel u and v. This was accomplished by utilizing the matrix2 option of the FSL probtractx software. A total of 50 independent components (ICs) in conjunction with the corresponding activation patterns in the brain space were computed in the gray matter voxel dimension by applying the Fast Independent Component Analysis (Fast ICA) algorithm to D_{uv} of each subject. The gray matter voxels that exhibited comparable structural connectivity patterns were identified and characterized as those components. These patterns were documented as DDTs of white matter at the voxel level, and subsequently compared to the WMATs observed in adult pigs[10].

Tract Comparison between adult pigs and piglets: Pearson correlation and KL-divergence

As illustrated in Figure 3.1B, both the Pearson correlation coefficient and the KL-divergence were employed to determine the similarity between the DDTs of piglets and the

WMATs of adult pigs. For the KL divergence, each DDT or WMAT was normalized and treated as a probability distribution. The symmetric KL divergence was calculated as follows:

$$KL_{ij} = \sum_n T_{in} log \frac{T_{in}}{W_{jn}} + \sum_n W_{jn} log \frac{W_{jn}}{T_{in}} \quad (3.1)$$

T_{in} quantifies the probability distribution for data-driven tract $\#i$ at voxel n, W_{jn} quantifies the distribution for WMAT $\#j$ at the same voxel n.

In our study, we matched each DDT with white matter atlas tract to discern structural similarities between piglet and adult pig brains. For each WMAT, we identified the DDT that exhibited the highest similarity by determining the lowest KL-divergence KL_{ij} among all 50 DDTs for each subject, where lower KL divergence indicating greater similarity. Concurrently, we calculated the spatial Pearson correlation coefficient matrix R between each DDT and WMAT, where, unlike KL divergence, a higher R_{ij} value signifies greater similarity, pinpointing the best-matching DDT for each WMAT. This procedure was applied consistently across all 11 subjects.

A threshold of 1-R = 0.7 (indicating a Pearson correlation > 0.3) was set as a criterion, alongside the consideration of KL-divergence and tract symmetry, for tract identification. For each WMAT, we selected and averaged the best corresponding component from each subject based on the highest Pearson correlation for visualization in Figure 3.4.

Unique Piglet tracts

This study also effectively identified unique piglet tracts using a purely data-driven approach. We utilized DDTs extracted from all 50 ICA components for each subject. These DDTs were compared across subjects independent of the WMATs. Our focus was on identifying specific DDTs demonstrating high Pearson correlation, with a set threshold of 0.6, consistently across a minimum of 9 out of the 11 subjects.

These correlated components were then aggregated and averaged to form a composite representation of each potential unique piglet tract. Subsequently, averaged tracts were compared against the 27 WMATs. Tracts exhibiting a Pearson correlation of less than 0.15 with any of the WMATs are considered unique tracts for piglets.

Extract and create connectivity Blueprint using common tracts

Following the identification of common tracts between adult pigs and piglets, we focused on symmetric cortical ROIs as outlined in Saikali's anatomical atlas [19]. These ROIs were selected based on their sufficiently large volumes, which are crucial for minimizing the potential misalignment issues during the co-registration process. Each of the 17 common tracts, in conjunction with the selected ROIs, was individually registered to every subject in our study. The registration process was necessary in developing a detailed connectivity blueprint, mapping structural connections in both piglet and adult pig brains. Figure 3.2A depicts a flow chart of this procedure. First, matrices of ROI by whole brain voxels and matrices of tract by whole brain voxels were generated using FSL Probabilistic Tractography (FSL probtractx) software. Next, ROI by tract matrices were calculated by matrix multiplication and recorded as voxel-based structural connectivity blueprints[18]. The blueprints were considered to contain connectivity information between each ROI and each identified tract. The approach was applied at the individual level, and a blueprint was generated for each subject of 11 piglets and 6 adult pigs, allowing for comparisons of between and within the two groups.

Comparing anatomical connectivity blueprints

The structural connectome blueprints in our study encapsulate the connectivity information between each ROI and the identified white matter tracts. As delineated in Figure 3.2B, we interpret the normalized rows of these blueprints as probability distributions. These distributions signify the

likelihood of each tract being connected to a specific ROI, as initially proposed by Mars, Sotiropoulos et al. [18]This interpretation stems from the fact that the blueprints are derived from probabilistic outcomes.

By utilizing the symmetric KL divergence, we can determine the similarity between the same ROI in different group subjects. The KL divergence for a given ROI KL_R between the piglet subject and adult subject is calculated by summing the divergence between the piglet blueprint P_{RT} and adult blueprint A_{RT} for each tract *T* using the following formula:

$$KL_R = \sum_T P_{RT} log \frac{P_{RT}}{A_{RT}} + \sum_T A_{RT} log \frac{A_{RT}}{P_{RT}} \quad (3.2)$$

This subject level results were calculated by pairwise comparing subjects within the piglet group ($n^2, n = 11$), subjects within the adult group ($N^2, N = 6$), and subjects across groups like shown in the equation ($n * N$). The results were recorded separately for each comparison.

Results

Data-driven tractography

Out of 27 WMATs of adult pig brains that revealed a high degree of correlation with human brains [10], 17 tracts that exhibited a high level of correlation with the DDTs of piglet brains. Highly consistent overlapping was found (over 90%) between the DDT indices with the highest Pearson correlation and the indices with the lowest KL-divergence out of the 50 independent components from the Fast ICA. This indicates a high degree of reliability and stability in the identified white matter tracts and the utility of comparing the two metrics. Table 1 lists the 17 tracts in detail[10].

Figure 3.3 presents the analytical results of symmetric KL-divergence and Pearson correlation (R). For comparison, we display 1-R values as blue boxplots and KL-divergence values as red solid boxplots. Both sets of boxplots indicate levels of dissimilarity. Our analysis highlights 17 tracts with a median correlation coefficient above 0.3, corresponding to 1-R values below 0.7.

These tracts also show a relatively low KL-divergence (around 8) and maintain symmetry between the left and right hemispheres. Figure 3.4 displays each tract, labeled according to the numbers listed in Table 1. The commonly found DDTs demonstrate significant symmetry between the left and right brain hemispheres, as evident in Figures 3.3 and 3.4. Specifically, tracts #7 and #8 (CBT_L and R) show extended tails penetrating the central white matter, highlighted by yellow arrows. This visualization emphasizes the distinct characteristics of the CBT tract in the piglet brain (refer to Table 3.1 for detailed tract information).

In our search for common tracts, we also identified a pair of bilateral tracts, labeled α1 and α2, and a self-symmetric tract, β1. The specific regions passed through by these tracts are detailed in Table 3.1, and visualizations of these tracts are shown in Figure 3.4. Notably, these three unique tracts each show a Pearson correlation of less than 0.15 when compared to any of the existing WMATs.

DDT comparison of gender difference

In our analysis, we computed the Pearson correlations between subjects for each of the 20 tracts. These correlations were then grouped by gender and subjected to an ANOVA test to determine significant differences between genders. Our findings indicate that no significant disparities were observed across any of the tracts based on genders. The most significant p value is 0.0584 for tract CST_R, which is slightly away from significant difference (See Table B2 for more details).

Structural blueprint comparison

The results of individual-level structural connectivity analysis are displayed in Figure 3.5, focusing on 52 (26 pairs of) gray matter ROIs on each hemisphere. These ROIs were chosen based on the anatomical symmetry and sizes and are detailed in Table B1. For all ROIs, the cross-group

(adult to piglet) KL-divergence values were significantly higher than within-group comparisons (adult to adult and piglet to piglet). Detailed p-values can be found in the Table B3. Notably, ROI pair #22 (Perirhinal cortex) showed the highest level of cross-group dissimilarity, as indicated by its highest mean KL-divergence value. Following closely were ROI pairs #21 (Anterior entorhinal cortex) and #23 (Parahippocampal cortex), each displaying unique structural connectivity patterns when compared across individual subjects.

Notably, the cross-group KL divergence values between adult pigs and piglets (AP group) were significantly elevated compared to the intra-group divergences of adult pigs (AA group) and piglets (PP group). This suggests a marked structural connectivity difference between the two age groups, while also indicating a higher degree of structural similarity within each group. Furthermore, the AP values exhibit notable bilateral symmetry, underscoring the robustness of the analysis. The ROIs with the highest AP values, indicating the greatest structural variability between adult pigs and piglets in three tracts, #22, #23, and #21.

Discussion

Tract and ROI similarity between piglet and adult pig group

Spatial correlation analysis revealed a high degree of structural connectivity similarity between piglets and adult pigs. Specifically, 17 out of 27 adult pigs' WMATs were found to exhibit a relatively high degree of spatial correlation or low KL divergence with DDTs identified in the piglet group. Of these 17 tracts, 16 (or 8 pairs) were found to exhibit symmetry across the left and right hemispheres. Only one cross-hemisphere tract was found. This symmetry serves as strong evidence of the reliability of the methodology.

Among the 27 WMATs, the results of the structural connectivity analysis revealed the presence of all projection tracts related to the thalamus, including the anterior thalamic radiation

(ATR), the corticospinal tract (CST), the optic radiation (OR), the posterior thalamic radiation (PTR), and the spinothalamic tract (STR). Furthermore, our analysis also identified four out of six tracts related to the visual cortex (i.e., the inferior fronto-occipital fasciculus (IFOF), the fornix (FMI), the optic radiation (OR), and the posterior thalamic radiation (PTR)), and three tracts related to the somatosensory and motor cortices (ATR, CST, and STR). This developmental difference in visual function was also noted in the KL-divergence-based connectome blueprint analysis (Fig.5), where the Perirhinal cortex, a critical part in processing both visual and auditory information, was found to be the mostly changed ROI between piglet and adult pig groups.

Based on the classification scheme proposed by previous studies [10,16], all projection tracts (ATR, OR, PTR, STR, and CST) were identified. For the commissural tracts [26], only the FMI was found. The fronto-occipital fasciculus (FMA) and middle cerebral peduncle (MCP) were absent. The association tracts showed the presence of IFOF and the uncinate fasciculus (UNC), but not the inferior longitudinal fasciculus (ILF). With regards to the limbic tracts, only the cingulum bundle (CBT) was identified, while the cingulum cingulate gyrus (CBD), cingulum parahippocampal gyrus (CBP), and fimbria (FX) were not observed.

Functionally, the commissural tracts play a crucial role in higher-level cognitive processes such as attention, language, and memory [27], while the limbic tracts, also known as the limbic circuitry, play a crucial role in regulating functions such as mood, motivation, memory, and autonomic functions[28]. The generally limited development of the commissural and limbic tracts is likely associated with differences in higher-level cognitive functions, such as memory and emotion, between the brain structures of piglets and adult pigs. These findings align with the developmental stages of the pig life cycle, where piglets first develop their motor system to compete with littermates to establish suckling teat ordered to compete for milk [29,30] and are capable

of standing and ambulating 15 minutes after birth. Vision and hearing are used in pre-weaning pigs, but these sensory functions are likely less critical in these early-stage animals. Similarly, higher-level cognitive functions like memory and emotion are clearly active in the early stages of a pig's life cycle as piglets establish teat order, identify siblings, and exhibit agnostic[31,32]. However, these high-level cognitive functions are likely to become further developed and more complex as animals age along with their associated brain structures such as the commissural and limbic tracts. This finding aligns with the blueprint study, which showed that the Anterior entorhinal cortex and Parahippocampal cortex — both crucial for memory processing — are the second and third most distinct ROIs between adult pigs and piglets. No significant differences were observed for the 20 piglet tracts (17 common and 3 unique tracts) between genders at the early age (3 weeks old) when their Pearson correlation with WMAT was examined with ANOVA. Further investigation should be conducted following different developmental stages in the future.

Data driven tract identification

We adopted a data-driven approach to identify unique tracts by analyzing DDTs derived from 50 ICA components for each subject, independent of WMATs. By setting a Pearson correlation threshold of 0.6, we pinpointed specific DDTs that consistently appeared in at least 9 out of 11 subjects. Notably, this methodology revealed over 20 tracts that met our high threshold and consistently appeared across the majority of piglets, underscoring the robustness and consistency of our findings within the subject population.

Individual-level cross group analysis

This study's individual-level analysis played a crucial role in examining the structural connectivity similarities between piglets and adult pigs. One of the primary advantages of this approach was the reduced boundary issues associated with registration procedures. By

necessitating fewer co-registration steps, the analysis likely achieved a higher level of accuracy, circumventing common challenges in registration processes. Another significant benefit of the individual-level analysis was enhanced statistical power. With a dataset of 6 adult pigs and 11 piglets, the study was able to conduct a wide range of inter- and intra-subject comparisons. This robust statistical approach was key in revealing both the differences and similarities in structural connectivity across and within different groups (Figure 3.5). The individual-level analysis effectively highlighted the variability in structural connectivity among different subjects. The marked difference in the cross-group KL-divergence values (referred to as 'AP' in Figure 3.5), in contrast to the intra-group comparisons ('AA' for adult pigs and 'PP' for piglets), accentuated the distinct structural characteristics between the two groups. It also underscored the significant degree of self-similarity within each group.

While the individual-level analysis offers several advantages, it also has limitations. This approach might not capture the broader trends and common features that could be more evident in a group-level analysis. Overall, the individual-level analysis provides critical insights into the nuanced aspects of structural connectivity in the brains of piglets and adult pigs, contributing significantly to our understanding in this field.

Gray matter mask generation

This study created the gray matter (GM) voxels by selecting the relevant areas from Saikali's anatomical atlas and then aligning these with each subject's voxels. This process, though practical, could lead to some mismatches between the brain structures of adult pigs and piglets, possibly introducing unexpected variables into our analysis. Alternatively, we also explored using FSL FAST segmentation to create a specific GM mask for each subject, aiming to tailor the analysis more closely to individual anatomies. However, when we compared the results from this

method with those from our original approach, we did not find significant differences in the DDT outcomes.

As a result, we kept our original method of aligning the atlas with each subject's voxels. This co-registration method provided richer anatomical details, which we deemed valuable for the depth and integrity of our study.

Voxel-based morphometry

The implementation of a voxel-based approach in our research presented the opportunity to leverage GM volume in calculating the whole brain matrix (GM* D_{uv}), as depicted in Figure 3.1, rather than relying on cortical surface area. This strategic pivot is particularly pertinent given the significant variability in cortical surfaces among subjects. However, it's crucial to note that distinguishing these variations demands high-resolution imaging, which is often not attainable with animal brain images. In scenarios where averaging is prevalent, such as in animal studies, registering to lower-resolution diffusion-weighted imaging (DWI) images can result in a notable loss of detail.

In this context, the voxel-based methodology offers a more pragmatic and valid approach for analyzing low-resolution pig models, particularly when co-registration is applied. This approach stands in stark contrast to surface-based methods, providing a more adaptable framework for handling the inherent challenges of low-resolution imaging.

Nonetheless, the voxel-based methodology has its limitations. The lower resolution of DWI images, especially acute in piglet brain imaging, presents significant challenges. This diminished resolution tends to obscure the demarcations between white and gray matter, as well as between gray matter and cerebrospinal fluid. Such ambiguity can lead to inaccuracies in segmentation, ultimately affecting the reliability and precision of the results. Therefore, while the voxel-based

approach mitigates some issues associated with low-resolution imaging, it is not immune to the intrinsic limitations that this imaging quality entails.

Limitations

Despite robust identification of structural tract similarities between piglets and adult pigs, this study is limited in several aspects and can be further improved upon. One such limitation is the use of 50 ICA components, which were repeatedly tested and refined, but may not be the optimal choice. This is because we found that several white matter tracts share the same best component, suggesting the possibility of combined tracts in these components. Additionally, the small sample size (N=11) of piglets in this study may also limit the statistical power of our results. In the future, larger sample sizes could provide a more robust assessment of these findings.

In conclusion, our data-driven approach has successfully established a comprehensive structural connectivity model for piglet brains, enabling ROI comparisons and effectively bridging the developmental gap between piglets and adult pigs. By unveiling 17 common white matter tracts and identifying 3 unique tracts specific to piglets, this study underscores the intricate structural parallels and distinctions within the porcine neurodevelopmental trajectory. The utilization of voxel-based methodology alongside independent component analysis enriches our understanding of piglet neuroanatomy, offering a robust framework for future translational neuroscience research. Notably, the comparative analysis between piglet and adult pig connectomes not only illuminates the developmental dynamics of neural pathways but also highlights the feasibility and significance of employing pig models for comprehensive, structural-guided neurodevelopmental studies. This work opens new avenues for exploring brain development and lays a solid foundation for subsequent investigations into the intricate mechanisms underlying neurodevelopmental processes.

Author Contribution

Wenwu Sun: Primary author of the article, contributed to the development of the methodology, data analysis and interpretation, and drafted the major portion of the article. Ishfaque Ahmed: contributed to data analysis and interpretation. Stephanie T. Dubrof: contributed to animal preparation and concept and preparation of experiment. Hea Jin Park, Franklin D. West, and Qun Zhao: contributed to concept and design of the study, development of the methodology, data interpretation, and finalization of article preparation.

Acknowledgement

This study was partially supported by the United States Department of Agriculture-National Institute of Food and Agriculture (Grant#: 2020-67017-30839)

Competing interest statement

None.

Declaration of generative AI and AI-assisted technologies in the writing process

During the preparation of this work the author(s) used Chatgpt in order to improve language. After using this tool/service, the author(s) reviewed and edited the content as needed and take(s) full responsibility for the content of the publication.

References

1. Xiong Y, Mahmood A, Chopp M. Animal models of traumatic brain injury. Nature Reviews Neuroscience 2013;14(2):128-142

2. Spear LP. Adolescent brain development and animal models. Annals of the New York Academy of Sciences 2004;1021(1):23-26

3. Simchick G, Shen A, Campbell B, et al. Pig brains have homologous resting-state networks with human brains. Brain connectivity 2019;9(7):566-579

4. Kinder HA, Baker EW, West FD. The pig as a preclinical traumatic brain injury model: current models, functional outcome measures, and translational detection strategies. Neural regeneration research 2019;14(3):413

5. Kaiser EE, West FD. Large animal ischemic stroke models: replicating human stroke pathophysiology. 2020;15(8):1377-1387, doi:10.4103/1673-5374.274324

6. Nakamura M, Imai H, Konno K, et al. Experimental investigation of encephalomyosynangiosis using gyrencephalic brain of the miniature pig: histopathological evaluation of dynamic reconstruction of vessels for functional anastomosis. Laboratory investigation. J Neurosurg Pediatr 2009;3(6):488-95, doi:10.3171/2008.6.PEDS0834 [pii]

10.3171/2008.6.PEDS0834

7. Kuluz JW, Prado R, He D, et al. New pediatric model of ischemic stroke in infant piglets by photothrombosis: acute changes in cerebral blood flow, microvasculature, and early histopathology. Stroke 2007;38(6):1932-7, doi:STROKEAHA.106.475244 [pii]

10.1161/STROKEAHA.106.475244

8. Tanaka Y, Imai H, Konno K, et al. Experimental model of lacunar infarction in the gyrencephalic brain of the miniature pig: neurological assessment and histological, immunohistochemical, and physiological evaluation of dynamic corticospinal tract deformation. Stroke 2008;39(1):205-12, doi:STROKEAHA.107.489906 [pii]

10.1161/STROKEAHA.107.489906

9. Baltan S, Besancon EF, Mbow B, et al. White matter vulnerability to ischemic injury increases with age because of enhanced excitotoxicity. The Journal of neuroscience : the official

journal of the Society for Neuroscience 2008;28(6):1479-89, doi:10.1523/JNEUROSCI.5137-07.2008

10. Benn RA, Mars R, Xu T, et al. A pig white matter atlas and common connectivity space provide a roadmap for the introduction of a new animal model in translational neuroscience. researchsquare 2020;2020, doi:https://doi.org/10.21203/rs.3.rs-105759/v1

11. Kinder HA, Baker EW, Wang S, et al. Traumatic brain injury results in dynamic brain structure changes leading to acute and chronic motor function deficits in a pediatric piglet model. Journal of Neurotrauma 2019;36(20):2930-2942

12. Simchick G, Scheulin KM, Sun W, et al. Detecting functional connectivity disruptions in a translational pediatric traumatic brain injury porcine model using resting-state and task-based fMRI. Scientific reports 2021;11(1):1-19

13. Fang X, Sun W, Jeon J, et al. Perinatal docosahexaenoic acid supplementation improves cognition and alters brain functional organization in piglets. Nutrients 2020;12(7):2090

14. Ahmed I, Reeves WD, Sun W, et al. Nutritional supplement induced modulations in the functional connectivity of a porcine brain. Nutritional Neuroscience 2023;1-12

15. Bryant KL, Ardesch DJ, Roumazeilles L, et al. Diffusion MRI data, sulcal anatomy, and tractography for eight species from the Primate Brain Bank. Brain Structure and Function 2021;226(2497-2509

16. Mars RB, O'Muircheartaigh J, Folloni D, et al. Concurrent analysis of white matter bundles and grey matter networks in the chimpanzee. Brain Structure and Function 2019;224(1021-1033

17. Warrington S, Bryant KL, Khrapitchev AA, et al. XTRACT-Standardised protocols for automated tractography in the human and macaque brain. Neuroimage 2020;217(116923

18. Mars RB, Sotiropoulos SN, Passingham RE, et al. Whole brain comparative anatomy using connectivity blueprints. Elife 2018;7(e35237

19. Saikali S, Meurice P, Sauleau P, et al. A three-dimensional digital segmented and deformable brain atlas of the domestic pig. Journal of neuroscience methods 2010;192(1):102-109

20. Wang M, Jiang J, Yan Z, et al. Individual brain metabolic connectome indicator based on Kullback-Leibler Divergence Similarity Estimation predicts progression from mild cognitive impairment to Alzheimer's dementia. European journal of nuclear medicine and molecular imaging 2020;47(2753-2764

21. Smith SM. Fast robust automated brain extraction. Human brain mapping 2002;17(3):143-155

22. Andersson JL, Sotiropoulos SN. An integrated approach to correction for off-resonance effects and subject movement in diffusion MR imaging. Neuroimage 2016;125(1063-1078

23. Behrens TE, Woolrich MW, Jenkinson M, et al. Characterization and propagation of uncertainty in diffusion-weighted MR imaging. Magnetic Resonance in Medicine: An Official Journal of the International Society for Magnetic Resonance in Medicine 2003;50(5):1077-1088

24. Jenkinson M, Bannister P, Brady M, et al. Improved optimization for the robust and accurate linear registration and motion correction of brain images. Neuroimage 2002;17(2):825-841

25. Behrens TE, Berg HJ, Jbabdi S, et al. Probabilistic diffusion tractography with multiple fibre orientations: What can we gain? neuroimage 2007;34(1):144-155

26. Tole S, Gutin G, Bhatnagar L, et al. Development of midline cell types and commissural axon tracts requires Fgfr1 in the cerebrum. Developmental biology 2006;289(1):141-151

27. Aralasmak A, Ulmer JL, Kocak M, et al. Association, commissural, and projection pathways and their functional deficit reported in literature. Journal of computer assisted tomography 2006;30(5):695-715

28. Alexander RP, Concha L, Snyder TJ, et al. Correlations between limbic white matter and cognitive function in temporal-lobe epilepsy, preliminary findings. Frontiers in aging neuroscience 2014;6(142

29. McBride G. The “teat order” and communication in young pigs. Animal Behaviour 1963;11(1):53-56, doi:https://doi.org/10.1016/0003-3472(63)90008-3

30. De Passille AMB, Rushen J. Suckling and teat disputes by neonatal piglets. Applied Animal Behaviour Science 1989;22(1):23-38

31. Clouard C, Resmond R, Prunier A, et al. Exploration of early social behaviors and social styles in relation to individual characteristics in suckling piglets. Scientific Reports 2022;12(1):2318

32. Hong J-K, Kim K-H, Hwang H-S, et al. Behaviors and body weight of suckling piglets in different social environments. Asian-Australasian Journal of Animal Sciences 2017;30(6):902

Common Tract	Description
ATR_L, R (#1,2)	Anterior Thalamic Radiation: connecting the thalamus with the prefrontal cortex
CBT_L, R (#7,8)	Temporal Cingulum: connecting the dorsal posterior cingulate and the parahippocampal cortex
CST_L, R (#9, 10)	Corticospinal Tract: connecting the brainstem and the sensorimotor cortex
FMI(#12)	Forceps Minor: connecting the left and right visual cortices passing through the splenium of the corpus callosum
IFOF_L, R (#15, 16)	Inferior Fronto-Occipital Fasciculus: connecting the visual and frontal cortex
OR_L, R (#20, 21)	Optic Radiation: connecting the thalamus with the inferior visual lobe
PTR_L, R (#22, 23)	Posterior Thalamic Radiation: connecting the thalamus to a V1 target mask
STR_L, R (# 24, 25)	Superior Thalamic Radiation: radiating from the thalamus to the primary and somatosensory association cortex
UNC_L, R (#26, 27)	Uncinate Fasciculus: connecting the anterior region of the inferior temporal gyrus into external capsule, terminating in the anterior prefrontal cortex

Unique Tract	Involved Anatomies
α1, 2	Caudate nucleus, Globus pallidus, Putamen, Substantia nigra, Anterior prefrontal cortex, Dorsal anterior cingulate cortex
β	Anteroventral thalamic nucleus, Mediodorsal thalamic nucleus, Ventral anterior thalamic nucleus, Fornix, Periaqueductal gray, Third ventricle, Cerebral aqueduct

Table 3.1. This table enumerates the 17 identified common white matter atlas tracts (WMATs), detailing the hemisphere location (L for left, R for right) and the corresponding number of tract# in Figure 3.3 (X-axis) and Figure 3.4. Additionally, this table includes information on the tracts that are unique to piglets and anatomies that these tracts pass through.

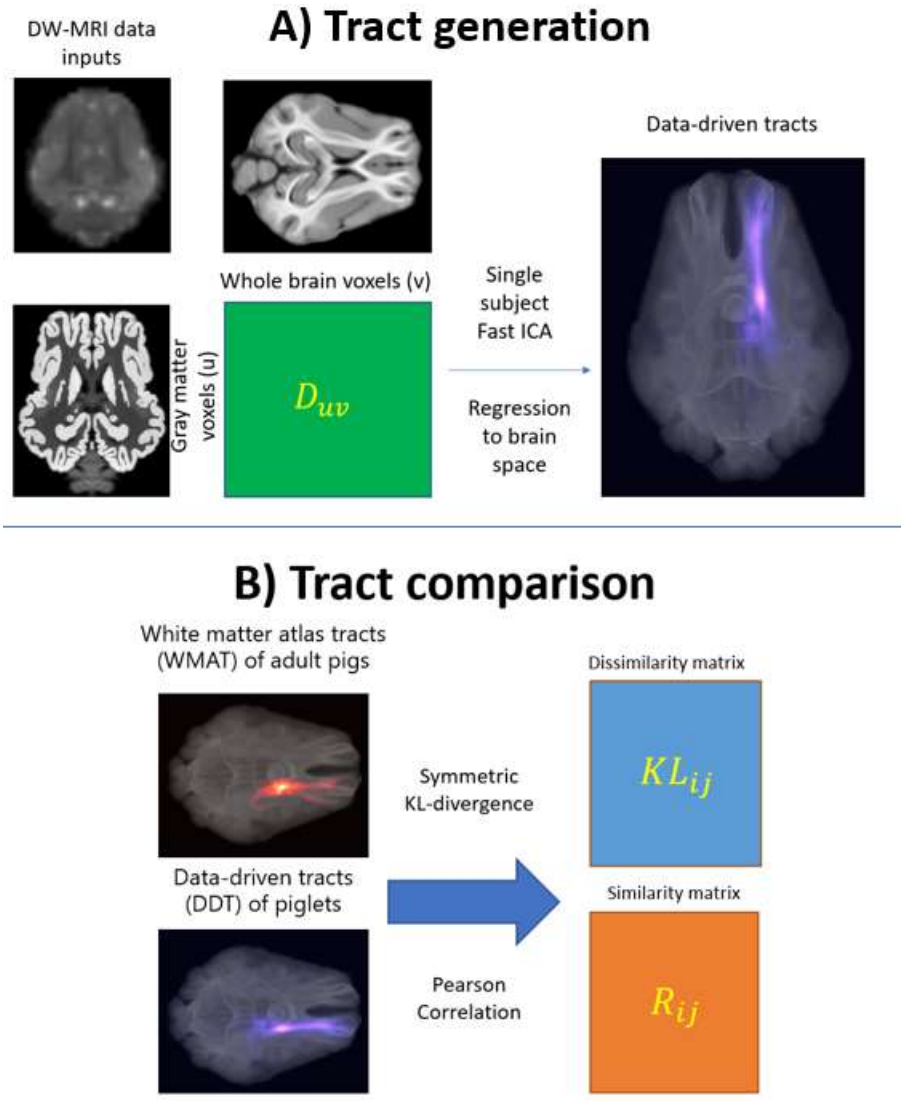

Fig.3.1 Flowchart of the voxel-based data-driven tractography analysis procedure. A) Tract generation: A gray matter (GM) atlas was first generated using the anatomical atlas (Saikali et. al). The number of simulated streamlines from GM voxels to whole brain voxels were then calculated using the DW-MRI data and collected as D_{uv} for each subject. The Fast

ICA and regression procedure was applied to D_{uv}, and patterns of every independent component (IC) were recorded as a DDT. B) Tract comparison of the WMAT and DDT: symmetric KL-divergence and Pearson correlation between each DDT with WMAT were calculated as KL_{ij} and R_{ij}.

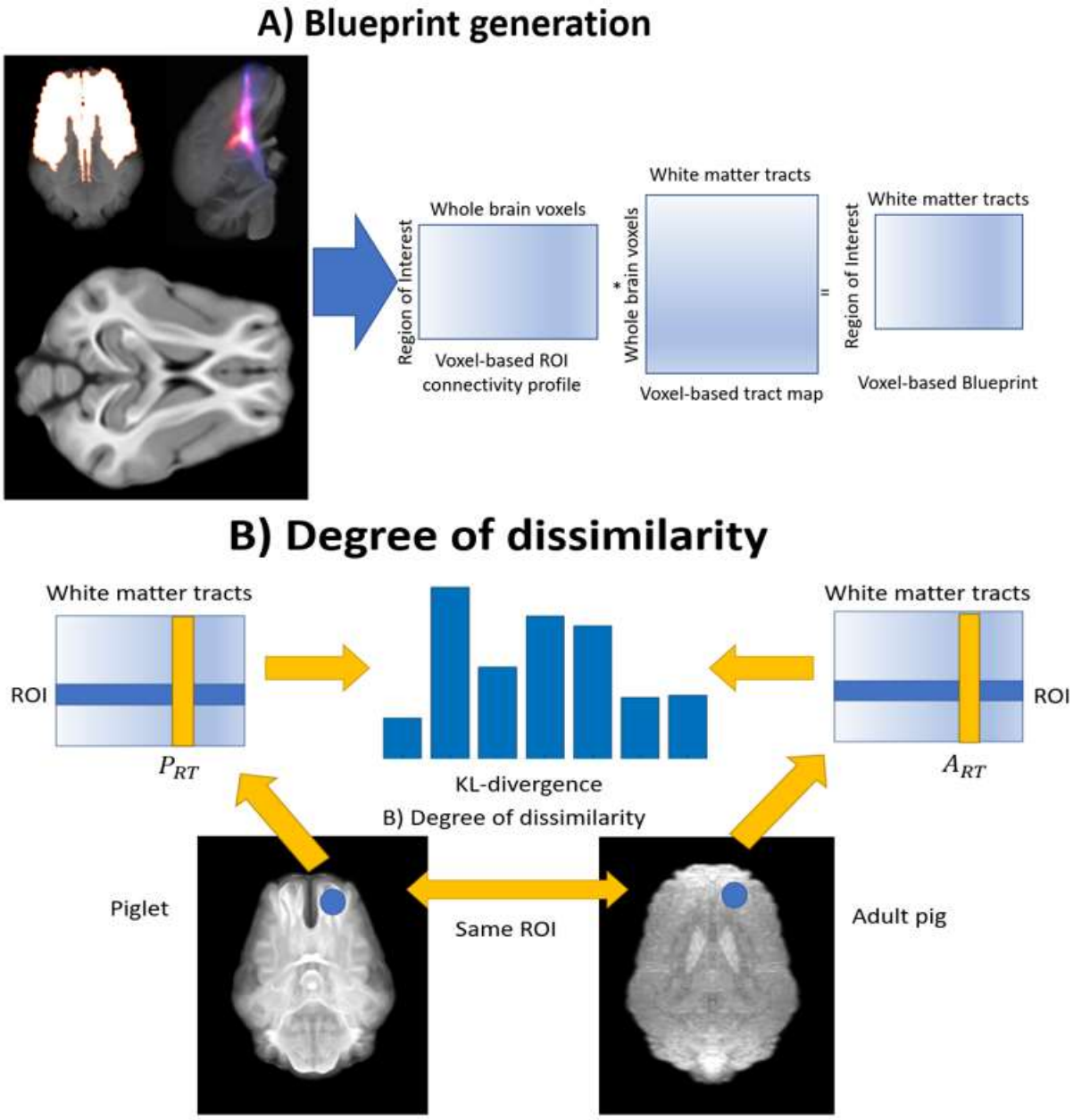

Fig.3.2 Flowchart of pig connectome blueprint generation and comparison. A) Blueprint generation: the procedure of creating voxel-based structural connectivity blueprints is conducted by generating matrices of region of interest (ROI) by whole brain voxels and matrices of tract by

whole brain voxels. B) Degree of dissimilarity: the rows of the generated connectivity blueprints of piglets (P_{RT}) and adult pigs (A_{RT}) are normalized and treated as probability distributions indicating the likelihood of each tract linking to a specific ROI. The dissimilarity between the ROIs in piglet and adult brains is then determined using the symmetric KL-divergence metric.

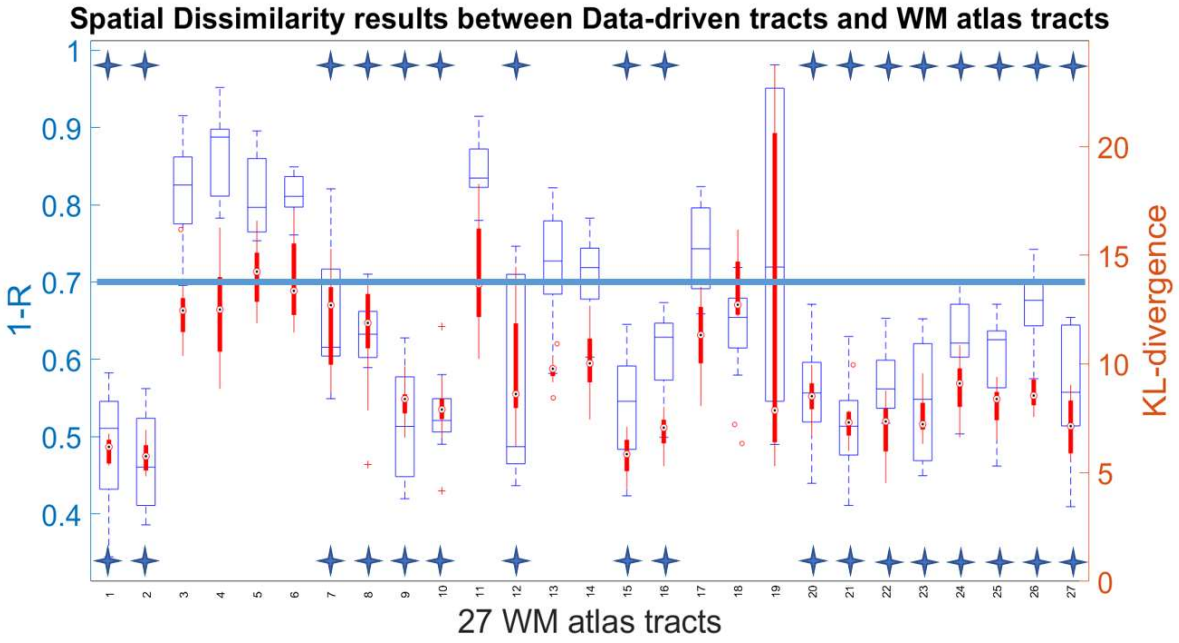

Fig.3.3 Comparative Analysis of Spatial Pearson Correlation and Symmetric KL-Divergence in WMATs and DDTs. The figure displays two types of boxplots: open, blue boxplots on the left, corresponding to the spatial Pearson correlation (1-R) on the left blue y-axis, and solid, red boxplots on the right, representing the symmetric KL-divergence between piglet DDTs and adult pig white matter atlas tracts (WMATs), aligned with the right red y-axis. A threshold of 1-R = 0.7 (indicating a Pearson correlation > 0.3) was set as a criterion, alongside the consideration of KL-divergence and tract symmetry, for tract identification. Out of 27 WMATs, 17 DDTs were identified that show a high level of similarity with their adult pig counterparts. Tracts meeting these criteria are marked with stars, and their specific white matter

atlas counterparts are enumerated in Table 1. Notably, symmetrically paired tracts demonstrated a significant resemblance to their corresponding atlas tracts.

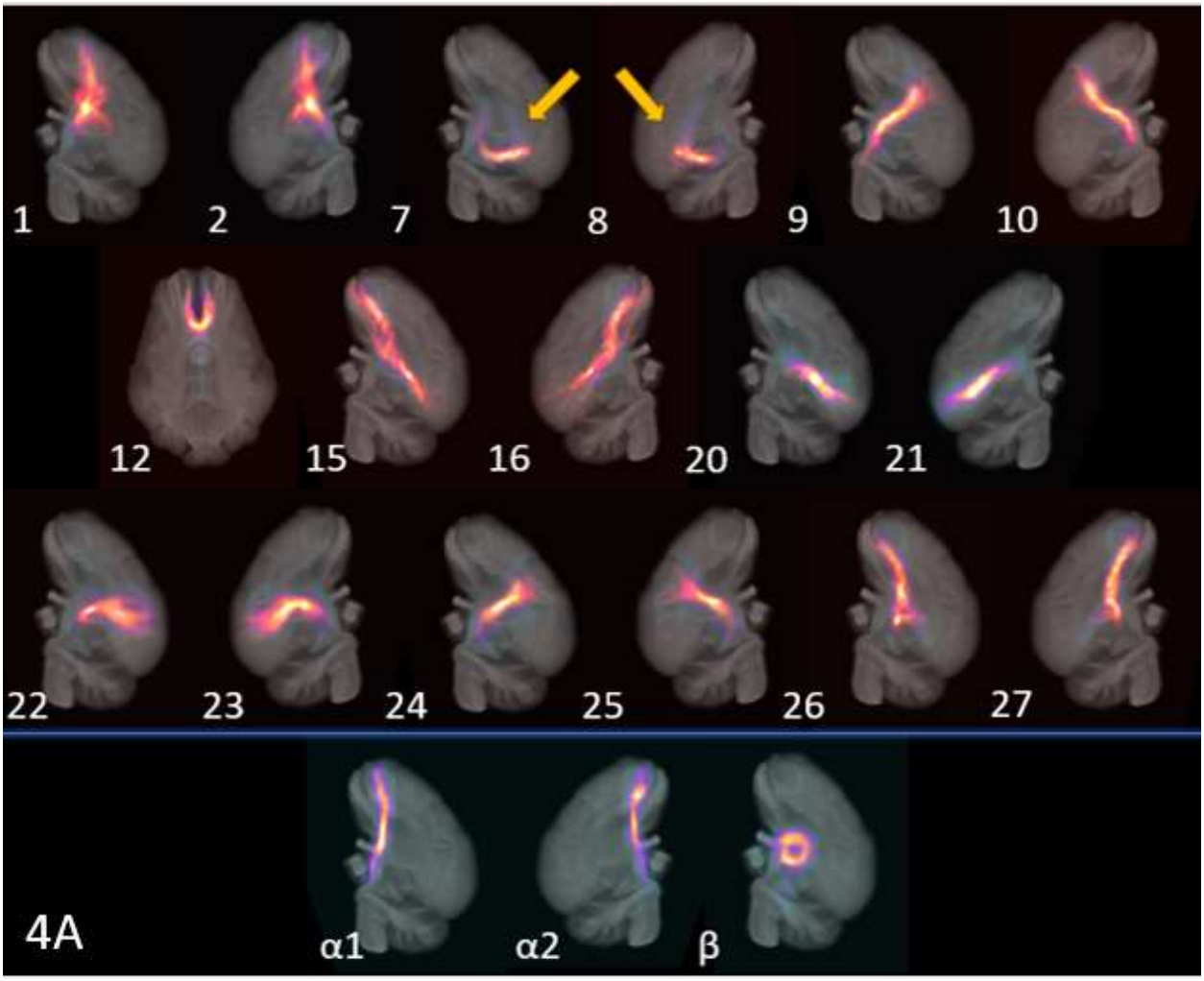
1
2
7
8
9
10
12
15
16
20
21
22
23
24
25
26
27
4A
α1
α2
β

4B

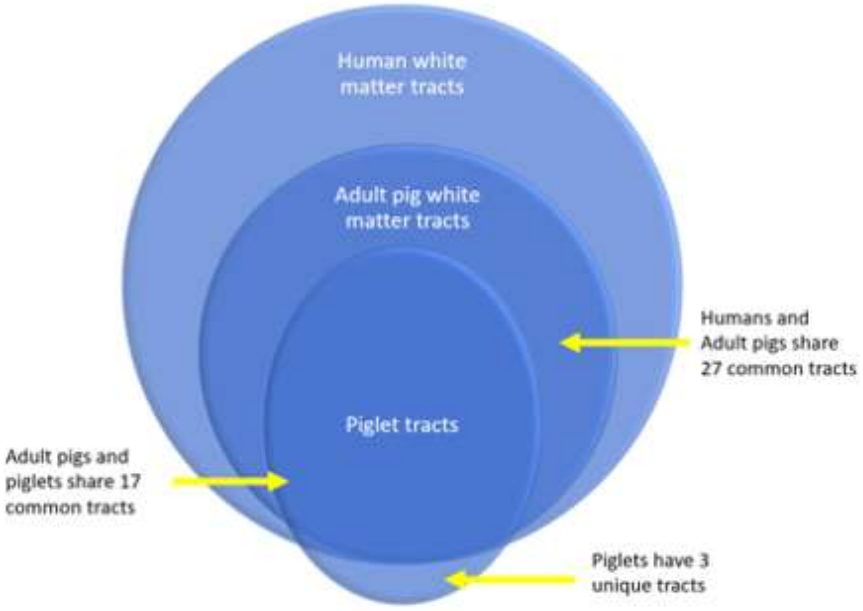
Human white matter tracts
Adult pig white matter tracts
Piglet tracts
Humans and Adult pigs share 27 common tracts
Adult pigs and piglets share 17 common tracts
Piglets have 3 unique tracts

Fig.3.4 Comparative Visualization and Tract Distribution Analysis. (4A): Subject-Averaged Data-Driven and Atlas-Based White Matter Tracts Visualization. The upper panel illustrates the overlaid tracts: data-driven tracts (depicted in purple) align closely with the white matter atlas tracts (in red), demonstrating significant similarity and bilateral symmetry. Tracts are labeled with numbers corresponding to those in Table 1 and Figure 3. Notably, as marked by yellow arrows, tracts #7 and 8 exhibit extended tails extending into the central white matter, underscoring the distinctive characteristics of the CBT tract in the piglet brain (refer to Table 1 for tract details). The lower panel reveals three piglet-specific tracts (in purple), representing average occurrences in at least 9 out of the 11 subjects and having a minimum Pearson correlation of 0.6. Comprehensive details and names of all tracts are provided in Table 1. (4B): Venn Graph of Tract Distribution. Figure 4B presents a Venn diagram illustrating the comparative distribution of tracts among humans, adult pigs, and piglets, offering a visual representation of the unique and shared tracts across the three groups.

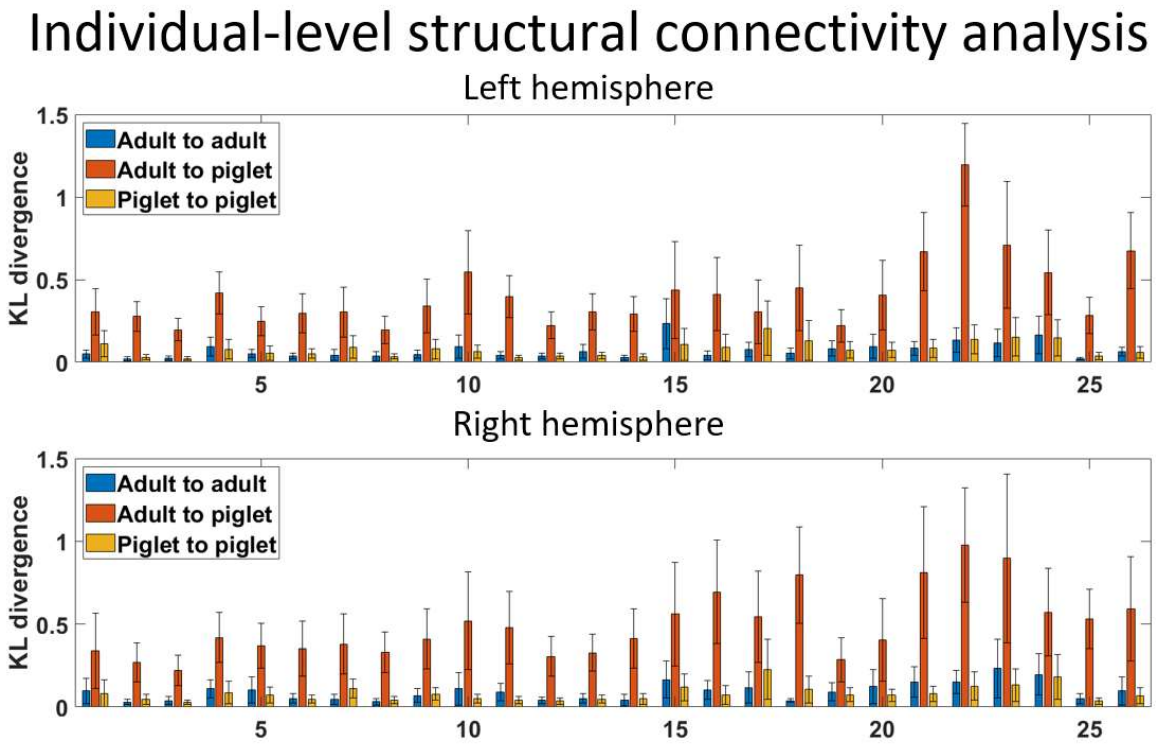

Fig.3.5 Results of Individual-Level Structural Connectivity Analysis Highlighting Cross-Group Differences. This figure is divided into two panels representing hemispheric differences in structural connectivity. The upper panel shows the results for the left hemisphere's regions of interest (ROIs), while the lower panel depicts those for the right hemisphere. The KL-divergence values across different groups are featured.

CHAPTER 4

INTEGRATING STRUCTURAL AND FUNCTIONAL BRAIN CONNECTIVITY: A MULTIMODAL FUSION APPROACH USING MACHINE LEARNING IN THE PORCINE MODEL[3]

[3] Sun, W., Ahmed, I., and Zhao, Q. To be submitted to *'Frontier in neuroscience'*

Abstract

Background

The exploration of brain connectivity presents a complex challenge in neuroscience, requiring advanced methodologies to understand the intricate interplay between structural and functional networks. The porcine model offers a valuable proxy for human neurological studies due to its similar neuroanatomical structure, including gyrencephalic brain and comparable white and gray matter distribution. This research builds on the necessity for multimodal data fusion, introducing a novel methodology, Connectome Matrix Fusion, to integrate structural connectivity (SC) and functional connectivity (FC) for a comprehensive analysis of brain dynamics.

Methods

This study utilized a cohort of 3-week-old piglets, divided into control and groups receiving different nutritional supplements (DHA, egg yolk, or both), to assess the impact of dietary interventions on brain connectivity. Employing T1-weighted MRI, resting-state fMRI, and diffusion-weighted MRI, we generated SC and FC matrices. The Connectome Matrix Fusion technique was developed, optimizing a parameter vector (R) through Covariance Matrix Adaptation Evolution Strategy (CMA-ES), to fuse SC and FC data on a nodal basis. The fusion's efficacy was evaluated using Support Vector Machine (SVM) classification, comparing the accuracy and confusion matrices against single-modality data.

Results

The application of Connectome Matrix Fusion yielded a significant improvement in classification accuracy, surpassing single-modality analyses by at least 15%. Notably, the

presence of crucial nodes across various classification tasks underscored the robustness of the global R vector, optimized to capture essential features across tasks.

Conclusion

The Connectome Matrix Fusion methodology demonstrated substantial potential in advancing neuroscience research, particularly using the porcine model. By successfully integrating SC and FC matrices, this approach has unveiled complex connectivity patterns within the brain, highlighting the efficacy of dietary interventions on neurological development. This study not only contributes to the body of knowledge in neuroimaging and brain connectivity but also opens avenues for future research into therapeutic interventions and the broader application of multimodal fusion techniques in neuroscience. Through the employment of advanced machine learning methods, including derivative-free optimization, this research underscores the versatility and depth of insights achievable with multimodal neuroimaging data, setting a new benchmark for neurological studies.

Introduction

Neuroscience research heavily relies on animal models, with the porcine model being particularly valuable due to its neuroanatomical parallels with humans. Structurally, this is evidenced by the proportionate distribution of white and gray matter, mirroring human brain development[1] [2]. Both pigs and humans share a gyrencephalic brain structure, crucial for intricate neural interconnections. Functionally, the porcine brain exhibits significant similarities to the human brain, reinforcing its applicability in translational research[3,4]. Recent studies in structural brain mapping have further aligned the pig brain with human neural architecture, enhancing the model's relevance for translational applications[5]. This confluence of structural and functional attributes allows for comprehensive investigations into the dynamics of structural connectivity

(SC) and functional connectivity (FC), with research increasingly integrating structural connectomes and functional regions of interest (ROIs) for deeper insights[6,7].

The rapidly advancing field of multimodal data fusion in brain imaging is revolutionizing our comprehension of brain structure and function. By integrating various imaging techniques such as diffusion tensor imaging (DTI) and functional MRI (fMRI), this approach offers a more holistic view of the brain's architecture and activity dynamics[8]. The synergy between structural connectivity and functional connectivity, crucial for understanding these dynamics, has been extensively documented[9].

The limitations of single modality studies become evident when examining complex neurodegenerative diseases like Alzheimer's. Here, multimodal fusion has proven pivotal in detecting both structural and functional brain changes, highlighting the inadequacy of relying solely on single imaging techniques[10,11]. This example underlines the broader necessity of multimodal studies in brain research, given the brain's intricate organizational principles and the need to explore beyond linear relationships between different data types.

Building on the demonstrated necessity of multimodal data fusion approaches, our study introduces an innovative methodology termed 'Connectome Matrix Fusion.' This technique synergistically combines SC and FC matrices, creating a unified connectome matrix, referred to as connectome matrix C. This integrated approach aims to provide a more comprehensive representation of brain connectivity by merging information from both SC and FC. By transcending the constraints of using SC or FC matrices separately, Connectome Matrix Fusion is designed to reveal latent patterns within the brain's connectome.

In our study, we applied this methodology to the porcine model, aiming to utilize diverse data sources for deeper insights. We assessed the method's efficacy in distinguishing healthy

control piglets from those subjected to various nutritional supplements, including Docosahexaenoic acid (DHA), egg yolk, or a combination of both. A notable outcome was the improved classification accuracy by at least 15% compared to single modality data, demonstrating the approach's effectiveness in revealing underlying connectivity patterns and its potential to significantly advance biomedical research.

Methods

Animal processing and data collection

In this investigation, we employed multi-modal neuroimaging techniques to acquire brain imaging data from 3-week-old piglets (n=44)[12]. The study encompassed four groups: a healthy control group (n = 14), a DHA-treated group (n = 12), an egg yolk-treated group (n = 12), and a group receiving both DHA and egg yolk supplements (n = 12). The imaging modalities included T1-weighted anatomical imaging, resting-state functional MRI (rs-fMRI), diffusion-weighted MRI (DW-MRI). The data collection was performed using a GE 32-channel Discovery MR750 3.0 Tesla magnet equipped with an 8-channel knee coil. All experimental procedures adhered strictly to the guidelines stipulated by the University of Georgia Institutional Animal Care and Use Committee (IACUC), under the approval number A2021 01-026.

Connectome matrix fusion

A flow chart for the Connectome Matrix Fusion method is shown in Figure 4.1. The fusion is performed with a parameter vector, R, to fuse the SC and FC data on a nodal basis. The core of our methodology lies in optimizing R through Covariance Matrix Adaptation Evolution Strategy (CMA-ES)[13-15]. This state-of-the-art optimization technique was pivotal in pinpointing the vector R that optimally interprets connectome information, thereby facilitating the best outcomes as evidence.

We evaluated the fusion performance using a Support Vector Machine (SVM) approach (Joachims 1998) to classify connectome matrices based on different nutritional supplements. The efficacy of the fusion was determined by comparing the accuracy and confusion matrices from this classification to those derived from individual SC and FC metrics. Our classification process involved a 3-fold cross-validation strategy and a comprehensive grid search for tuning SVM hyperparameters—specifically, the regularization parameter, kernel type, and kernel coefficient—according to changes in vector R. Detailed descriptions of these methodological advancements are presented in the subsequent sections.

Data Preprocessing

The input dataset contains SC and FC matrices, which are characterized by distinct physical nature and scales. In order to render them comparable and facilitate their fusion, appropriate data preprocessing is necessary. The FC matrices were utilized in their original form of partial correlation without modification. On the other hand, the SC matrices were preprocessed using a logarithmic transformation to manage the different scaling of the distribution of functional and structural connectivity strengths. This transformation enhances the robustness of the subsequent analyses, ensuring a more reliable and accurate interpretation of the connectome data [11]. The transformation to SC matrices is followed by the addition of a small epsilon to address zero-values within the data.

Time-resolved functional connectivity

We have limited availability of subjects in our initial dataset—comprising merely 12 or 14 subjects in each group. This scarcity of data poses some challenges, primarily related to the model's susceptibility to overfitting and its ability to generalize well to unseen data. To enhance the diversity and richness of our dataset, we incorporated the concept of time series

segmentation[16] to augment our dataset. In our approach, we extracted shorter time series segments from the original resting state functional MRI (rs-fMRI) time series, and treated the segmented times as added individual subjects. Specifically, we extracted segments of 150 time points from the original 300 time points long series. By shifting 30 time points at a time, we constructed a new subject, ultimately forming six distinct subjects out of the original one. To mitigate the challenges posed by potential class imbalances within the data, we employed a custom Synthetic Minority Over-sampling Technique (SMOTE) function designed for 3D data[17].

However, there is a possibility that this technique might introduce the risk of data leakage due to the inherent overlap between the constructed subjects. To carefully mitigate this risk and maintain the integrity of our cross-validation process, all six augmented subjects derived from the same original subject were allocated exclusively to the same training or testing set during the following 3-fold validation evaluation. This ensured that our evaluation metrics were not over-optimistic and provided a reliable and robust assessment of our model's performance.

Connectome Matrix Fusion

Our fusion protocol is designed to integrate the distinct yet complementary data from SC and FC matrices. The aim is to create a composite connectome matrix, referred to as C, which is expected to surpass the classification accuracy of SC or FC matrices alone and improve the depiction of brain connectivity patterns. This method involves a weighted linear combination governed by a vector R, whose dimensionality matches the number of nodes in the matrices. It merges corresponding rows and columns from SC and FC matrices to form C. This fusion technique is uniformly applied across all subjects, ensuring uniformity in the application of the vector R.

The method is mathematically represented as:

$$C_{s,i}^{r} = R_i \cdot SC_{s,i} + (1 - R_i) \cdot FC_{s,i} \qquad (4.1)$$

$$C_{j,s}^{c} = R_j \cdot SC_{j,s} + \left(1 - R_j\right) \cdot FC_{j,s} \qquad (4.2)$$

$$and\ C = C^r + C^c \qquad (4.3)$$

Here, $M_{s,i}^{r}$ $(M, a\ matrix\ representing\ C, SC, or\ FC)$ represents the i^{th}node (row) of the s^{th} subject, and $M_{j,s}^{c}$ represents the j^{th}node (column) of the s^{th} subject.

While the edges (correlation between a pair of nodes) of FC matrices are inherently symmetric and commutative, depicting undirected associations or relationships, the edges of SC matrices from node I to node J and their counterparts (from node J to I) inherently exhibit asymmetry, reflective of the directional nature of structural connections. Given the innate directional asymmetry in SC edges, we opted to process them symmetrically to refrain from the introduction of external information. However, we intentionally preserved the inherent asymmetry stemming from SC to keep the embedded, directional information within the fused matrices.

Classification and hyperparameter tuning

The classification efficacy of the fused connectome matrices was evaluated using a Support Vector Machine (SVM) to distinguish between variations in brain development resulting from different nutritional supplements. To mitigate the risk of variance in our small dataset and enhance the robustness of our findings, a stratified K-fold cross-validation approach with three folds was employed. The SVM was fine-tuned through a comprehensive grid search across a spectrum of hyperparameters, which were adapted in response to variations in the R vector to optimize classification performance. These parameters included the regularization constant, choice of kernel, and its associated coefficient, as delineated in the supplementary materials. The mean classification accuracy, calculated over the three folds for each hyperparameter set,

informed the optimization of the R vector. The procedure is shown on the right side of the Fig.1 flowchart.

Optimization of R using CMA-ES

Our objective was to refine the vector R to enhance classification accuracy. We employed the CMA-ES, a non-derivative optimization method, due to its efficacy in high-dimensional, non-linear functions. CMA-ES is well-suited for complex optimization problems, with its vast parameter space.

CMA-ES operates by dynamically adjusting a multivariate normal distribution, using a mean vector and covariance matrix. Each iteration produces new candidate solutions from this distribution, which are evaluated to inform adjustments to the distribution's parameters. This adaptive approach aims to direct the search towards optimal regions within the parameter space, circumventing the need for gradient information. The gradient-free characteristic of CMA-ES is particularly beneficial for optimizing functions that are non-convex, non-smooth, or noisy. Its ability to navigate through irregular objective functions makes it robust for identifying optimal R values. A flowchart of CMA-ES procedure is shown in Figure 4.1.

Specifically in our study, CMA-ES aims to locate the optimal combination of R values that fuses the most distinguished connectome information and therefore generates the highest classification accuracy. We defined a bound constraint for the R values, limiting them between 0 and 1 [11]. The optimization process was configured to take early stopping when the function value changes were too small, ensuring the achievement of a near-optimal solution. Additionally, a maximum of 200 iterations were allowed to maintain computational efficiency. The optimization process was initialized with an initial guess for the R values as a vector with all elements set to 0.5, representing an equal contribution of structural and functional connectivity matrices in the

fused matrix initially. The initial standard deviation was set to 0.2 to allow a sufficient exploration of the solution space in the initial phase of the optimization. The CMA-ES optimizer was then run with the cross-validation function, which encapsulated the classification model, as the objective function to be minimized.

Task-specific and global R for optimization accuracy

In our analytical framework described above, an R vector is specifically optimized for each specified task, focusing on binary classification among the control group and the three distinct nutrition study cohorts (DHA, Egg Yolk, and combo group). This task-specific R vector is crafted to accentuate the features embedded within both SC and FC. We have also instituted a global R (GR) vector that is globally applied to the three binary tasks. Its aim is to ascertain an optimized R vector with universal applicability across a spectrum of tasks, thereby establishing a standard benchmark for comparative analyses. This global approach not only mitigates the risk of overfitting but also serves as a testament to the method's robustness.

The pursuit of a GR vector involves the optimization of average classification accuracy over a trio of binary classification tasks between the control group and each of the respective nutrition study groups. To validate the consistency of our method, both the task-specific and GR vectors were subjected to multiple optimization iterations. We have employed a fixed random seed 42, a widely recognized standard, across most aspects of our study except for CMA-ES procedures. This approach ensures reproducibility and maintains consistency in accuracy when solely employing SC and FC for comparative assessments. Results obtained under varying random seeds have demonstrated comparable robustness, further substantiating the reliability of our findings. Details of these results are available upon request.

Results

The accuracy for each task is shown in Table 4.1. for the GR task, the shown accuracies are averaged among the three binary tasks. The significant nodes (thresholded by 0.12) is shown in figure 4.2. Specifically, an R value that approaches 1 implies a predominant role of SC in the fusion, signifying that the structural information of a particular node is consistently crucial for the classification of brain states or conditions. An R value nearing 0 indicates a predominance of FC, suggesting that for these nodes, the functional aspects of connectivity exert a greater influence on the classification outcomes.

In the results of our analysis, we observed a significant overlap in the nodes identified as crucial for classification in the individual tasks of Combo, Egg, and DHA to the control group with those identified in the GR task. This intersection of node significance underscores the robustness of the GR vector which was optimized to capture the essential features required across the various tasks. More than 65 percent nodes in the DHA to control (6 out of 9), Egg yolk to control (6 out of 9), and Combo to control tasks (12 out of 15) are found to overlap with the GR task crucial nodes. Furthermore, more than 85 percent of crucial nodes identified in the GR task also showed up in three single tasks (18 out of 21). Specifically, GR overlaps with DHA task with the following nodes [*#4 Hippocampus, #29 Putamen, #32 Primary_Somatosensory_Cortex, #39 Primary_visual_cortex, #46 Dorsal_anterior_cingulate_cortex, #49 Parahippocampal_cortex*], overlaps with Egg yolk task with these nodes [*#10 Dorsolateral_prefrontal_cortex, #13 Primary_visual_cortex, #14 Secondary_visual_cortex, #25 Auditory_Cortex, #28 Caudate_nucleus, #45 Dorsal_posterior_cingular_cortex*], and overlaps with Combo task with nodes [*#3 Putamen, #4 Hippocampus, #20 Dorsal_anterior_cingulate_cortex, #32 Primary_Somatosensory_Cortex, #35*

Premotor_Cortex, #37 Anterior_prefrontal_cortex, #39 Primary_visual_cortex, #43 Middle_temporal_gyrus, #45 Dorsal_posterior_cingular_cortex, #46 Dorsal_anterior_cingulate_cortex, #48 Perirhinal_cortex, #49 Parahippocampal_cortex]. On the other hand, while there's only one overlap node between the Egg yolk and the combo tasks, more than half crucial nodes in DHA (nodes [#*4 Hippocampus, #32 Primary_Somatosensory_Cortex, #39 Primary_visual_cortex, #46 Dorsal_anterior_cingulate_cortex, #49 Parahippocampal_cortex*]) occurred in Combo task. Those five nodes also occurred in the GR group, potentially marking the effect of the DHA supplement in brain development.

Discussion

Comparison between baseline and the fusion

A crucial part of our evaluation was to confirm that the classification accuracy achieved through the optimized R vectors surpasses the accuracy of using solely SC or FC. Through the employment of fusion connectomes, we observed a substantial enhancement in accuracy across all tasks, exhibiting increments exceeding 15% for each of the tasks. The enhancement in classification accuracy proved the efficiency of our methodology, indicating that the incorporation of both SC and FC information, optimized through R, contributes to a more comprehensive and accurate representation of connectivity patterns.

Global R: Balancing Variance and Bias

Incorporating a global R within diverse tasks served as a mechanism to moderate variance whilst maintaining minimal bias in our study. In the context of machine learning, variance refers to the model's sensitivity to fluctuations in the training dataset, whereas bias refers to the error introduced by approximating complex real-world problems with simplified

models. High variance normally is related to underfitting and unstable results among datasets, while high bias normally is related to overfitting, and the model is addicted to the training dataset. The deployment of a global R constraint is purposed to force the model to discover more intrinsic, underlying patterns that are inherent in the data.

As shown in the result section, more than 65% of nodes in the separate tasks are shown in the GR tasks as crucial nodes, which account for more than 85% of nodes in the GR task. The presence of these nodes in the GR task demonstrates the model's ability to assimilate and prioritize features that are consistently influential across diverse datasets. This consistency not only reaffirms the validity of the globalized approach but also indicates these nodes as potential biomarkers for further investigation into brain connectivity distinctions between different dietary interventions.

DHA classification with high overlap and lowest accuracy: good or bad?

Our study reveals a good overlap between the DHA task and the combo task, where both DHA and egg yolk are used as food supplement to the piglets. More than half crucial nodes in DHA task appeared in the combo task, while only 1 overlap node was found between the egg yolk and combo tasks. This finding may suggest the dominance of DHA effect in brain development shown by those shared crucial nodes, while egg yolk does not have consistent effect on those brain regions. However, a consistent pattern of lesser accuracy in the task of delineating between DHA group with the control group, whether utilizing SC, FC, or the fused connectome approach. This trend also appears in the global R study. When the global R is applied to the tasks, the DHA classification task still holds the least accuracy. This consistent observation of comparably low classification accuracy irrespective of the computational approach employed may suggest a potential minimal differentiation between the control and

DHA groups. Such uniformity in accuracy patterns may be indicative of a more subtle inter-group distinction.

Utilization of CMA-ES: A Derivative-Free Method

In our study, we employed Covariance Matrix Adaptation Evolution Strategy (CMA-ES), a derivative-free optimization method, owing to its unique advantages and capabilities. One notable advantage of employing CMA-ES is its ability to allow for a clear, dual-staged procedure, enabling the retention of the Support Vector Machine (SVM) in its original form while separately conducting the optimization. This distinct separation significantly alleviates the computational burden during training, which is a crucial factor considering the constraints of our dataset's size. The derivative-free nature of CMA-ES also offers capability for problems where the objective function is stochastic, noisy, or discontinuous, which enabled us to search for the best SVM hyperparameters to apply. Specifically, in stochastic settings where output variability is influenced by randomness, CMA-ES, with its population-based approach, ensures a robust performance, as it does not depend on gradient information and thus is not misled by the randomness. Similarly, in scenarios with noisy function evaluations, the algorithm's ability to average out noise over multiple evaluations and generations grants it a significant edge over gradient-based methods, which might otherwise struggle due to inaccurate gradient computations. In cases of discontinuous objective functions, where gradients might not be defined or can exhibit abrupt changes, CMA-ES stands out as it navigates based on the ranking of solutions, not their gradient values. This aspect is particularly beneficial when searching for optimal SVM hyperparameters, as the performance landscape with respect to these parameters can be intricate, displaying noise and discontinuities, especially with a limited dataset. Furthermore, its inherent capacity to explore the global search space methodically enhances its

potential to locate optimal solutions that gradient-based methods might overlook, especially in the presence of multiple local optima.

However, the non-gradient nature of CMA-ES presents its own set of challenges. The absence of gradient descent imposes limitations on the precise interpretation and justification of the optimization procedures, potentially complicating the explanation of the resultant optimal solutions. This can often lead to a complex navigation through the solution space and might necessitate additional justification to corroborate the optimization path undertaken.

In summary, while the lack of gradient information in CMA-ES necessitates interpretation of optimization trajectories, its ability to efficiently reduce parameters to learn, navigate through complex solution spaces and its adaptability to diverse problem scenarios render it an invaluable tool, particularly when addressing challenges with smaller datasets and non-differentiable objective landscapes.

Data leaking

Within the framework of our study, special emphasis was placed on circumventing any form of data leakage to ensure the integrity and validity of our results. Data leakage is a critical concern as it can lead to overly optimistic evaluations and compromises the generalizability of the model to unseen data. To rigorously prevent such mishaps, we took great care of organization of our datasets, particularly focusing on the segregation of augmented data. Each augmented data, regardless SC or FC, was kept in its entirety within distinct folds, ensuring a stringent partition between training and testing sets in every fold of our model's evaluation. This arrangement precluded any cross-contamination of information between the training and testing phases, preserving the sanctity of the independent testing environment and thereby fortifying the robustness of our evaluation metrics.

Randomness in the study

In our study, we acknowledged the multifaceted role of randomness in to balance both the robustness and replicability of our findings. The selection of the random seed is pivotal in controlling the stochasticity inherent in our methodologies, and we consciously elected a well-accepted starting point, random seed value of 42, for most components entailing random processes, except for the CMA-ES optimization. This deliberate choice provided dual advantages: first, by allowing the randomness inherent in CMA-ES optimization, we introduced an element of robustness into our investigation, and second, by maintaining a consistent random seed in other components, we ensured that our results were reproducible and transparently traceable. It is imperative to underline our cognizance regarding the potential misuse of random seed selection to inflate results, a practice we stringently avoided. Our approach was not to cherry-pick a seed that would present our work in a disproportionately favorable light, but rather to illustrate the inherent robustness of our methods.

In conclusion, the comprehensive evaluation of Connectome Matrix Fusion within this study underscores its substantial potential in advancing neuroscience research, particularly in the context of the porcine model. By successfully integrating structural and functional connectivity matrices, this innovative approach has demonstrated a notable enhancement in classification accuracy, thereby confirming its efficacy in capturing the intricate connectivity patterns of the brain. The employment of machine learning methods, including the derivative-free optimization technique CMA-ES, has further enriched our analytical toolkit, allowing for the robust evaluation of complex neuroimaging data without the constraints of traditional gradient-based optimization. Our findings revealed the impact of dietary interventions on brain connectivity and also pave the way for future investigations into the fusion between structure and function within

the brain. As we continue to unravel the complexities of brain connectivity, the insights garnered from this study provide a promising foundation for exploring therapeutic interventions and deepening our understanding of neurological development and recovery processes.

References

1. Spear LP. Adolescent brain development and animal models. Annals of the New York Academy of Sciences 2004;1021(1):23-26

2. Kuluz JW, Prado R, He D, et al. New pediatric model of ischemic stroke in infant piglets by photothrombosis: acute changes in cerebral blood flow, microvasculature, and early histopathology. Stroke 2007;38(6):1932-1937

3. Kinder HA, Baker EW, West FD. The pig as a preclinical traumatic brain injury model: current models, functional outcome measures, and translational detection strategies. Neural regeneration research 2019;14(3):413

4. Simchick G, Shen A, Campbell B, et al. Pig brains have homologous resting-state networks with human brains. Brain connectivity 2019;9(7):566-579

5. Benn RA, Mars R, Xu T, et al. A pig white matter atlas and common connectivity space provide a roadmap for the introduction of a new animal model in translational neuroscience. researchsquare 2020;2020, doi:https://doi.org/10.21203/rs.3.rs-105759/v1

6. Mars RB, Sotiropoulos SN, Passingham RE, et al. Whole brain comparative anatomy using connectivity blueprints. Elife 2018;7(e35237

7. Sun W. Evaluation of traumatic brain injury in pigs using a novel cross-group temporal correlation analysis. London; 2022.

8. Damoiseaux JS, Greicius MD. Greater than the sum of its parts: a review of studies combining structural connectivity and resting-state functional connectivity. Brain structure and function 2009;213(525-533

9. Honey CJ, Sporns O, Cammoun L, et al. Predicting human resting-state functional connectivity from structural connectivity. Proceedings of the National Academy of Sciences 2009;106(6):2035-2040

10. Tong T, Gray K, Gao Q, et al. Multi-modal classification of Alzheimer's disease using nonlinear graph fusion. Pattern recognition 2017;63(171-181

11. Zhang L, Wang L, Gao J, et al. Deep fusion of brain structure-function in mild cognitive impairment. Medical image analysis 2021;72(102082

12. Fang X, Sun W, Jeon J, et al. Perinatal docosahexaenoic acid supplementation improves cognition and alters brain functional organization in piglets. Nutrients 2020;12(7):2090

13. Hansen N, Auger A. CMA-ES: evolution strategies and covariance matrix adaptation. 2011.

14. Loshchilov I, Hutter F. CMA-ES for hyperparameter optimization of deep neural networks. arXiv preprint arXiv:160407269 2016;

15. Varelas K, Auger A, Brockhoff D, et al. A comparative study of large-scale variants of CMA-ES. Springer: 2018.

16. Zalesky A, Fornito A, Cocchi L, et al. Time-resolved resting-state brain networks. Proceedings of the National Academy of Sciences 2014;111(28):10341-10346

17. Chawla NV, Bowyer KW, Hall LO, et al. SMOTE: synthetic minority over-sampling technique. Journal of artificial intelligence research 2002;16(321-357

Task	Accuracy with SC (%)	Accuracy with FC (%)	Accuracy with fused connectome (%)
Control – DHA	58.3±2.2	59.0±2.1	83.8±1.3
Control – EGG	70.8±3.8	70.8±2.0	93.0±1.8
Control – combo	75.0±4.0	68.8±2.3	93.5±1.0
GR	68.0±4.2	66.2±3.8	84.6±0.3

Table 4.1: Classification accuracies for various tasks using structural connectivity (SC), functional connectivity (FC), and a fused connectome. Accuracies for SC and FC are determined with a fixed seed ensuring reproducibility, while fused connectome results are the average of 10 trials (8 trials for GR), and all results are further averaged across three folds. The fused connectome achieves superior performance as seen in each binary classification task (along each row), particularly showing the highest accuracy (93.5%) in the Control – combo task, whereas the Control – DHA task demonstrates the lowest accuracy (83.8%). Notably, the GR task maintains a comparable accuracy in the fused connectome condition as to the binary classification tasks (along each column).

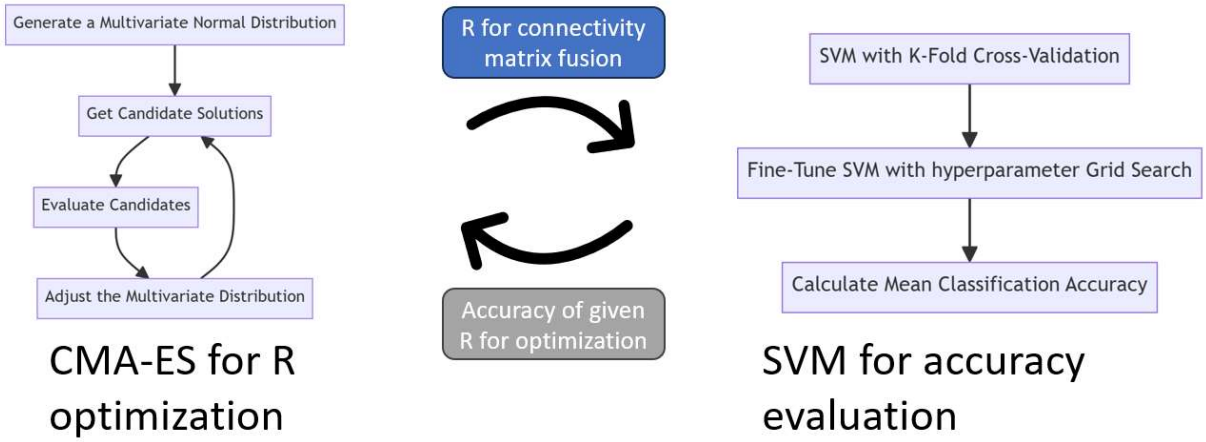

Figure 4.1: Integrated Workflow of Covariance Matrix Adaptation Evolution Strategy (CMA-ES) and Support Vector Machine (SVM) Classification Processes: This graph illustrates the operation of two advanced computational methodologies. On the left, the CMA-ES procedure is depicted, showcasing its iterative cycle of generating candidate solutions, evaluating them, and adjusting the distribution parameters. This process efficiently explores the parameter space to find optimal solutions. On the right, the SVM classification process is outlined, demonstrating its use in binary classification (in this case, distincting brain development influenced by nutritional supplements) through a stratified K-fold cross-validation approach and hyperparameter optimization. The iterative fine-tuning of the SVM, informed by mean classification accuracy, complements the adaptive search strategy of CMA-ES, together providing a comprehensive framework for the evaluation of fusing parameter R.

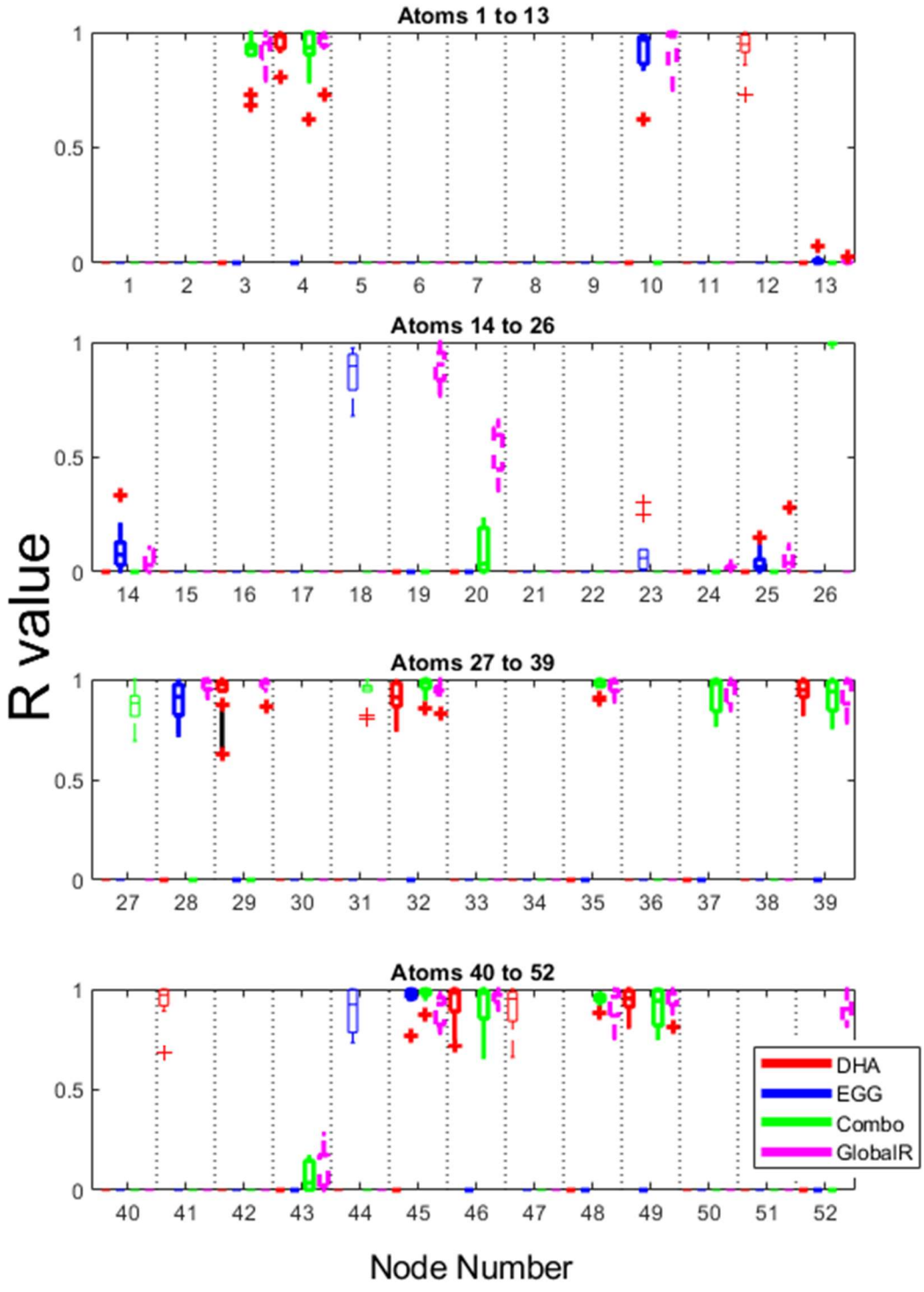
Atoms 1 to 13
Atoms 14 to 26
Atoms 27 to 39
Atoms 40 to 52
R value
Node Number
DHA
EGG
Combo
GlobalR

Figure 4.2: Illustration of crucial nodes in classification task in GR, DHA, Egg yolk and Combo group. The R vectors acquired from different tasks were compared and are depicted in the illustrative boxplot, with each task uniquely colored for clear delineation. In this illustration, emphasis is placed solely on nodes that persistently exhibit a predominant influence (thresholded with a standard deviation less than 0.12) thereby serving as crucial determinants in the classification tasks. Nodes manifesting considerable variance within each task's R vectors are treated as non-crucial for the corresponding task and are not shown to enhance visualization clarity. An R value approaching 1 signifies a dominance of SC in the fusion process, highlighting that the SC information of this particular node is consistently pivotal for classification tasks. Conversely, an R value near 0 underscores the dominance of FC, indicating that the functional aspects of connectivity are more influential in the classification process for that node.

CHAPTER 5

CONCLUSIONS

The core narrative of this dissertation revolves around the innovative use of MRI to bridge structural and functional connectivity study in the brain. This dissertation employs the pig brain as a viable surrogate for human brain study. Through temporal fMRI analysis, we gained insights into the dynamic processes of brain recovery post-TBI, emphasizing the importance of a baseline for comparison. Moving forward, spatial DTI allowed us to map the structural connectivity in piglets, revealing both similarities and unique aspects when compared to adult pigs. This exploration into structural connectivity laid the groundwork for the final leap - the fusion of connectome matrices. The Connectome Matrix Fusion methodology exemplified the power of integrating multiple data modalities to achieve a holistic understanding of brain connectivity.

In chapter 2 of this research, we employed the pig model to study traumatic brain injury (TBI)—a leading cause of death and long-term disability worldwide. Our research introduces a new designed methodology for temporal analysis of functional magnetic resonance imaging (fMRI) data, aimed at evaluating the recovery of brain function post-TBI. This innovative approach is distinct from conventional analyses in its utilization of a cross-group correlation analysis between TBI-affected subjects and a sham group that underwent craniotomy surgery only and without TBI induction. Current studies normally use several metrics and compare the TBI group results to the sham/control group results, while we used the correlation between TBI and sham as the metric for evaluating the TBI recovery effect. This deep evolvement of the sham

group as a correlation baseline for normal functional connectivity is unprecedented in TBI research, enabling a comparison of recovery trajectories while accounting for variables such as the effects of surgical intervention and natural aging.

By incorporating both sparse dictionary learning (sDL) and independent component analysis (ICA) for the extraction of time series of resting-state networks (RSNs), our analysis delivers a more sophisticated understanding of the temporal dynamics of brain recovery post-TBI. Furthermore, the integration of cerebral blood flow (CBF) maps into our analysis not only underscores the reliability of our method in tracking recovery but also reinforces the alignment between cerebral perfusion and functional connectivity patterns. Such a methodological framework is vital for the field, as it addresses a crucial part in existing TBI research: evaluation, by providing a rigorous mechanism to assess and compare the efficacy of therapeutic interventions over time.

Our study's key contributions are highlighted by the experimental findings that revealed a consistent increase in correlation between the fecal microbial transplant (FMT) treated group and the sham group within the executive control and salience networks, indicating the effectiveness of FMT as a post-TBI treatment. Additionally, a simulation designed to mimic the progression of TBI severity underscored the decreasing temporal correlation between sham and TBI groups with increasing injury severity, consistent with our experimental observations. These results not only validate the efficacy of our novel methodology in evaluating post-TBI treatments but also contribute significantly to the field by opening new avenues for future investigations into TBI treatment evaluations.

Then in Chapter 3 of this doctoral exploration, we investigated the structural connectivity of the brain using DTI. We pioneered the creation of a white matter atlas tract (WMAT) model

tailored for piglets, revealing 17 tracts that are consistent with those found in adult pigs, and additionally identifying three tracts unique to piglets. This achievement bridges the gap in our understanding of structural brain development across different life stages and also illuminates the distinct structural intricacies inherent to the piglet brain. Such insights are instrumental in advancing our comprehension of neurodevelopmental trajectories and the mechanisms underlying brain recovery following injury.

Our research introduced a voxel-based structural connectivity (SC) analysis, employing ICA on diffusion-weighted magnetic resonance imaging (DW-MRI) data derived from piglets. Our approach represents a significant methodological leap departing from traditional surface-based analyses to embrace a voxel-based paradigm. By doing so, we were able to harness the granularity of voxel-based data, allowing for the generation of data-driven tracts (DDT) that very well capture the complex organization of the brain with unprecedented detail. The effectiveness of voxel-based SC ICA in this context is particularly notable, demonstrating an unparalleled capacity to unravel the intricate structural connectivity within the developing piglet brain.

Another focus in our methodological framework was the application of structural connectome blueprints, a concept that facilitated a comprehensive mapping of the brain's structural networks. The consistent result in positive and negative markers of tracts and highly different ROIs between piglets and adult pigs both revealed possible development pattern of the porcine model.

The significance of our findings extends well beyond the immediate scope of this study, laying a foundational cornerstone for future neuroscience research. By establishing the first WMAT model for piglets, our work opens new pathways for exploring brain development, offering a template for investigating the effects of various interventions on neurodevelopmental

outcomes. Furthermore, the methodological innovations introduced in this chapter—namely, the voxel-based SC analysis and the use of structural connectome blueprints—equip researchers with powerful tools for dissecting the complex architecture of the brain. This comprehensive approach to mapping structural connectivity in piglets not only enriches our understanding of neurodevelopmental processes but also sets the stage for a deeper exploration of the potential impacts of therapeutic interventions on brain structure and function.

Finally, in Chapter 4 of this doctoral research, we embarked on an ambitious journey to transcend traditional boundaries in brain imaging, harnessing the synergistic potential of Connectome Matrix Fusion. This groundbreaking methodology, which seamlessly integrates structural connectivity (SC) and functional connectivity (FC) matrices into a unified connectome matrix, represents a leap in our quest to decode the intricate coupling of the brain's connectivity. Drawing on the profound anatomical and functional parallels between porcine and human brains, Connectome Matrix Fusion emerges as a transformative approach in neuroscience, enabling a holistic and nuanced exploration of brain architecture and activity.

Our pioneering application of Connectome Matrix Fusion is predicated on the understanding that the multifaceted complexity of brain connectivity transcends what can be captured through single-modality imaging studies alone. By coupling SC and FC data, we construct a comprehensive connectome matrix that embodies the full spectrum of brain connectivity, offering invaluable insights into the underlying patterns of neural interaction and organization. This integrative technique is particularly crucial in differentiating different states of the brain where it facilitates a more robust detection than using only structural and functional brain alterations, thereby providing a more complete framework for evaluating brain changes.

The practical application of our Connectome Matrix Fusion methodology within the porcine model has yielded significant findings, particularly in differentiating healthy control piglets from those subjected to various nutritional interventions, including Docosahexaenoic acid (DHA), egg yolk, or a combination of both. The improved classification accuracy by at least 15% over traditional single modality approaches underscores not only the methodological robustness of Connectome Matrix Fusion but also its profound efficacy in uncovering latent connectivity patterns that lie beyond the reach of conventional imaging techniques. This achievement highlights the methodology's broad applicability and its potential to revolutionize biomedical research, opening new avenues for investigating and understanding the brain's connectome with unparalleled depth and precision.

Based on these studies, the new methodologies pave the way for a comprehensive future study of TBI. We have developed the sham-base metric for evaluation of the TBI effect on the functional part, which can be readily adapted for structural comparisons. Through the development of the SC ICA method, we have successfully identified tracts in both piglet and adult pig brains, opening avenues for in-depth aging and developmental studies within the pig model. This approach is particularly advantageous for conducting long-term investigations into the effects of TBI. Additionally, the identified tracts serve as valuable markers for determining ROIs, further refining our analysis.

Building on these advancements, we plan to apply our methodologies to a newly created fused connectome matrix. This will allow us to uncover intrinsic patterns within the brain, facilitating a thorough understanding of TBI recovery mechanisms. By integrating functional and structural data through our novel techniques, we aim to gain comprehensive insights into the

dynamics of TBI recovery, setting the groundwork for future research in this critical area of neuroscience.

In conclusion, this PhD research represents a significant stride towards a more integrative and comprehensive understanding of the brain's structural and functional complexities. By leveraging the pig model as a surrogate for human brain studies, we have unveiled new dimensions of brain connectivity, recovery, and the potential for therapeutic interventions.

APPENDIX A

SUPPLEMENTARY MATERIALS – CHAPTER 2

Temporal correlation analysis

In our research, we first adopted a temporal correlation approach to examine the similarities in brain temporal activity between corresponding RSN nodes in the brains of the sham group and those undergoing TBI (SLN or FMT group). To accomplish this, we innovatively adapted the FSLNets tool, which was initially developed for comparing connectivity strength between different RSN nodes. Specifically, we modified FSLNets to assess the correlation of activity within the same RSN node across different individuals—one from a TBI group and another from the sham group—thereby creating a 'pseudo subject'. Generation of pseudo subjects allows FSLNets to identify correlations in node activity between the sham and TBI groups over time.

The process involves several steps: First, we paired time series from corresponding nodes of subjects in a TBI group with those in the sham group, concatenating these series to form a 2-dimensional matrix (2K by t) that simulates a single subject with twice the number of nodes (2K) for analysis by FSLNets. Second, using FSLNets' functions, we calculated correlation matrices for these 2K nodes, which were then transformed into temporal Z-score matrices via Fisher's transformation. A one-group T-test assessed the null hypothesis of no correlation, producing Z-stats that were interpreted within the context of our study's adapted FSLNets pipeline. Next, from these matrices, we specifically focused on the Z-stats between corresponding nodes across the TBI and sham groups, shown as the diagonal red blocks at the lower-left quadrant of the correlation

matrix (right section of Figure A1). These Z-stats, which traditionally gauge temporal functional similarity, were repurposed in our study to measure recovery or disruption in resting-state networks (RSNs) following TBI.

Spatial correlation analysis

The masked 3D CBF maps associated with each RSN were rearranged into 1D arrays (i.e., in the same format as time series) and then analyzed using the same FSLNets functions as in temporal analysis. Similar to the temporal correlation analysis, we aligned rearranged CBF data from the TBI group and the sham group to generate pseudo subjects, forming data matrices with dimensions 2K by v, where v is the number of voxels for the RSN in the ASL space. We then calculated inter-node correlation coefficient matrices for each RSN at both time points (D1 and D7). To reduce any potential bias in the cross-group correlation analysis, we conducted drop-one-out tests using 128 randomized group tests.

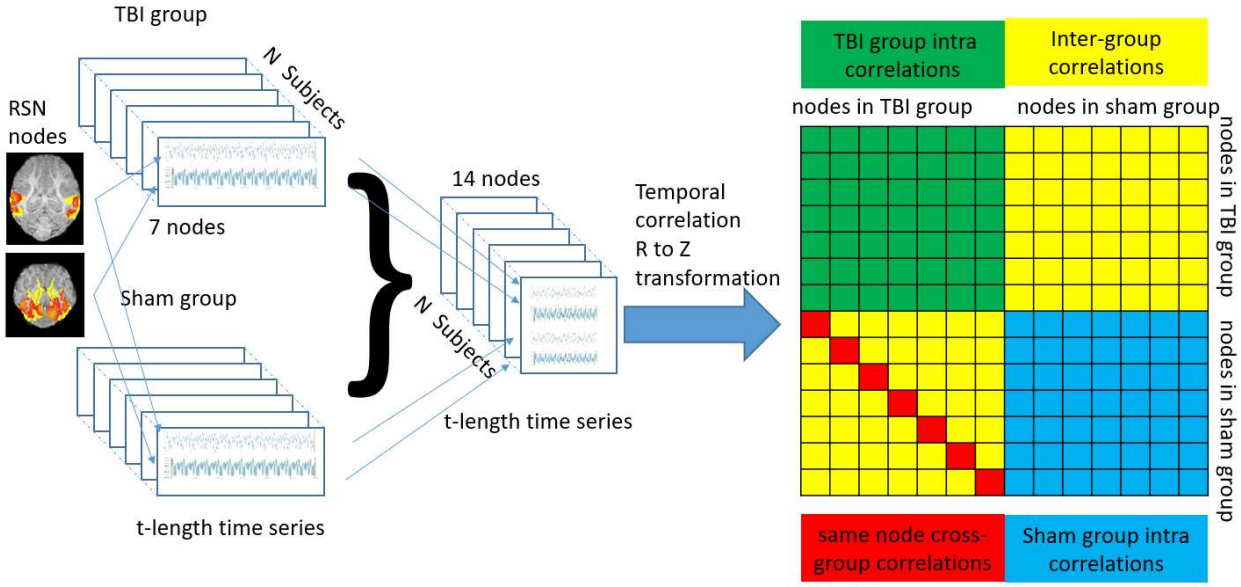

Figure A1: Flowchart depicting the cross-group temporal analysis methodology. Time series are rearranged to form pseudo subjects, doubling the node number for FSLNets functions. In the FSLNets' node by node matrix output, the red diagonal of the yellow matrix represents inter-group correlations between the same nodes. These red diagonals are collected and treated as similarities between nodes' behaviors in different groups.

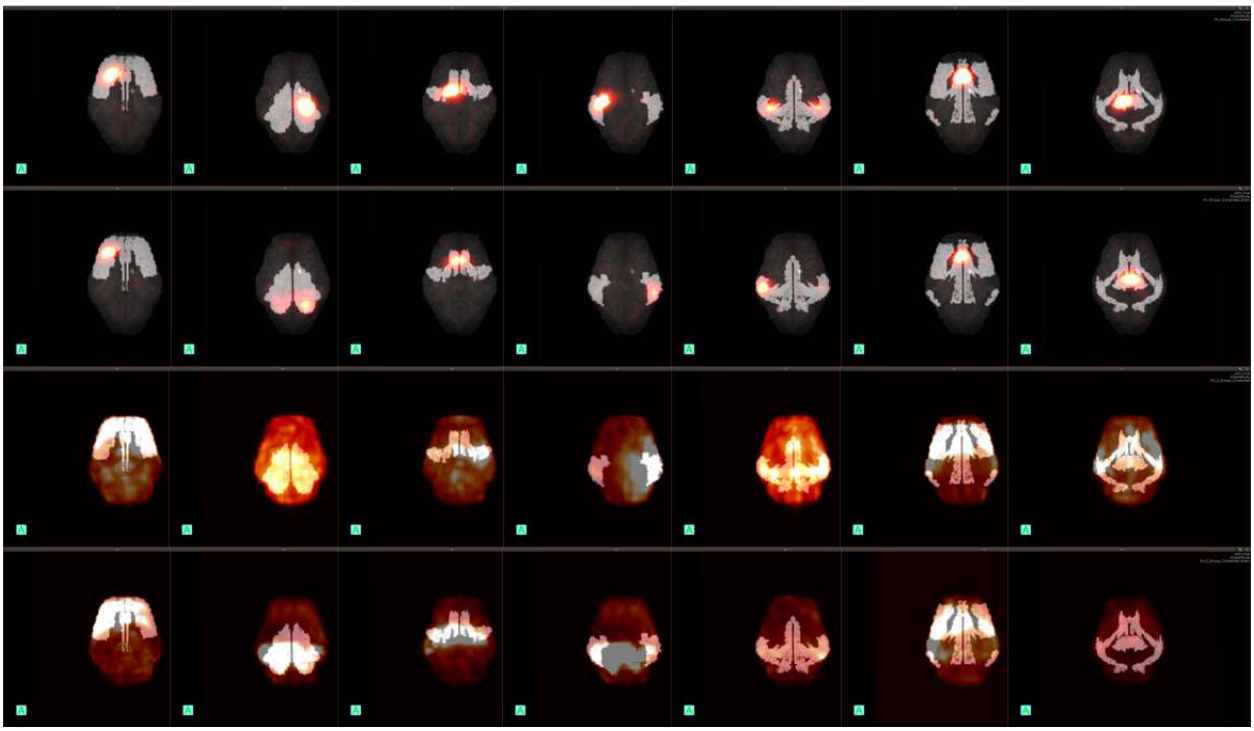

Figure A2. Visualization of overlapping each RSN's atlas with the best correlated node from ICA and sDL group learning that was employed in the study. Columns from left to right represent RSNs: EXN, VIS, SMN, DMN, AUD, SAL, and BAS; rows from top to bottom: ICA with FL (full dataset learning), ICA with SL (sham-only dataset learning), sDL with FL, and sDL with SL. It is seen that the ICA nodes are more condensed and independent from each other, while the sDL nodes have larger distribution across the brain. The ICA nodes' activation maps are usually only part of the RSN, while the sDL can fill most of the atlases. In ICA, no consistent clear difference can be observed between the FL and SL results. In sDL, SL shows more symmetric results in SMN and AUD, while other RSNs remain at a similar level in symmetry.

APPENDIX B

SUPPLEMENTARY MATERIALS – CHAPTER 3

Supplementary Materials

#	anatomy
1	Ventral anterior thalamic nucleus
2	Caudate nucleus
3	Putamen
4	Hippocampus
5	Amygdala
6	Primary Somatosensory Cortex
7	Primary Motor Cortex
8	Somatosensory Association Cortex
9	Premotor Cortex
10	Dorsolateral prefrontal cortex
11	Anterior prefrontal cortex
12	Insular cortex
13	Primary visual cortex
14	Secondary visual cortex
15	Associative visual cortex
16	Inferior temporal gyrus
17	Middle temporal gyrus
18	Superior temporal gyrus
19	Dorsal posterior cingular cortex
20	Dorsal anterior cingulate cortex

21	Anterior entorhinal cortex
22	Perirhinal cortex
23	Parahippocampal cortex
24	Fusiform gyrus
25	Auditory Cortex
26	Prepyriform area

Table B1. Name of the 26 symmetric pairs of ROIs selected in the study.

Negative white matter tracts for piglets	Description
CBD_L, R	Cingulum Dorsal Bundle: connecting the dorsal posterior cingulate and the border of the anterior and posterior cingulate cortex.
CBP_L, R	Pregenual Cingulum: connecting the dorsal anterior cingulate to anterior prefrontal cortex passing the genu of the corpus callosum
FMA	Forceps Major: connecting the left and right visual cortices passing through the splenium of the corpus callosum
FX_L, R	Fornix: connecting the corpus callosum and the hippocampus and amygdala
ILF_L, R	Inferior Longitudinal Fasciculus: connecting the inferior temporal gyrus to the inferior occipital lobe
MCP	Middle Cerebellar Peduncle: connecting the left and right cerebellar peduncles

Table B2. Name and information of 10 negative white matter tracts for piglets, present in the adult pig brain only.

Tract number#	P-value
1	0.636976
2	0.55287
7	0.320605
8	0.797284
9	0.721022
10	0.058384
12	0.709753
15	0.783491
16	0.695009
20	0.339079
21	0.828006
22	0.325993
23	0.782321
24	0.789842
25	0.793411
26	0.238168
27	0.722846
α1	0.804011
α2	0.139509
β	0.107583

Table B3. This table lists the identified piglet brain white matter tracts with their ANOVA p-values, crucial for evaluating gender-based connectivity differences. No significant differences were found.

Region of interest number#	Adult to adult versus piglet to adult results	Piglet to piglet versus piglet to adult results
1	5.04E-19	5.98E-26
2	3.44E-31	0
3	5.74E-29	0
4	2.11E-27	0
5	7.38E-25	0
6	5.37E-24	0
7	7.88E-18	8.31E-30
8	2.35E-20	0
9	5.88E-19	1.64E-37
10	1.08E-18	0
11	1.18E-30	0
12	4.17E-25	0
13	3.26E-23	0
14	5.11E-28	0
15	1.59E-05	1.27E-23
16	2.92E-17	2.74E-33
17	6.39E-11	2.18E-05
18	3.52E-15	1.92E-24
19	1.66E-13	2.20E-30
20	1.71E-14	1.56E-39
21	1.98E-27	0
22	2.80E-45	0
23	1.52E-15	3.19E-34
24	1.95E-14	5.30E-34
25	1.37E-26	0
26	2.55E-29	0
27	2.29E-09	1.61E-23
28	8.75E-22	0
29	2.03E-21	0
30	6.37E-22	0
31	8.95E-20	0
32	9.04E-19	0
33	1.93E-19	5.52E-35
34	6.10E-27	0
35	1.07E-19	0
36	2.72E-13	2.97E-41
37	9.37E-19	0
38	2.31E-24	0

39	1.94E-27	0
40	3.38E-22	0
41	6.59E-12	1.14E-33
42	4.56E-20	0
43	1.90E-15	5.56E-19
44	8.56E-29	0
45	2.12E-14	4.23E-38
46	3.76E-10	3.80E-33
47	5.69E-17	0
48	2.37E-26	0
49	2.55E-12	2.35E-37
50	9.08E-14	4.22E-30
51	1.07E-29	0
52	1.26E-15	1.21E-42

Table B4. This table displays the differences in structural connectivity blueprints via ANOVA testing. The second column shows p-values for adult-to-adult versus cross-group (adult pig and piglet) connectivity, while the third column indicates p-values for piglet-to-piglet versus cross-group connectivity. All comparisons reveal significant intra-group differences compared to inter-group results.